Evolutionary remodeling of non-canonical ORF translation in mammals

Yue Chang[1,2], Tianyu Lei[1,2], Feng Zhou[1], Jiawen Jiang[1], Yu Huang[1], Ziyang Zhu[1], Hong Zhang[1*]

[1]College of Ecology, Lanzhou University

[2]These authors contributed equally

[*]Correspondence: hong_zhang@lzu.edu.cn (H.Z.)

Abstract

Non-canonical open reading frames (ncORFs) are pervasive within transcripts annotated as "non-coding" or "untranslated regions" of mRNAs, yet their landscape under normal physiological conditions remains to be fully resolved, particularly outside humans. Here we applied a stringent and standardized pipeline to hundreds of high-quality ribosome profiling libraries from normal mammalian tissues and cell types, identifying 11,623 human and 16,485 mouse ncORFs. Evolutionary analyses revealed that thousands of ncORFs are subject to coding constraint and exhibit lineage-specific conservation, underscoring their functional potential. Ancient ncORFs are preferentially highly translated, broadly expressed, and enriched for lineage-specific conservation. Co-expression patterns further indicate that many ncORFs, especially ancient ones, are cotranslated with canonical coding sequences, consistent with functions mediated through protein–protein interactions. Together, these findings establish a comprehensive atlas of mammalian ncORFs and provide fundamental insights into their evolutionary dynamics and functional integration within the proteome.

Keywords: non-canonical open reading frame; annotation; translation; evolution; mammals.

Introduction

The systematic identification of functional genomic elements represents a foundational objective in the field of genomics. Among these elements, non-canonical open reading frames (ncORFs)—which are open reading frames (ORFs) located within long non-coding RNAs (lncRNAs) or untranslated regions (UTRs) of mRNAs—have attracted considerable attention in recent years[1-5]. While certain ncORF subtypes, such as upstream ORFs (uORFs) located in 5' UTRs and downstream ORFs (dORFs) in 3' UTRs, have been extensively characterized for their ability to regulate mRNA translation and stability in *cis*, a growing body of evidence demonstrates that ncORFs can also give rise to functional proteins that engage in diverse cellular pathways[1,2,6,7]. As functional ncORFs continue to be discovered across multiple eukaryotes[8-17], systematic elucidation of their composition and function promises to uncover an additional layer of regulatory complexity and to refine our conception of the so-called "non-coding" genome.

Although ncORFs may play important biological roles, the number of translated ncORFs in the human genome remains uncertain. Detection by mass spectrometry (MS)-based proteomics is challenging, likely due to their short lengths and low abundances[18]. Ribosome profiling (Ribo-Seq) offers greater sensitivity for identifying translation events[18,19], but downstream computational pipelines often produce highly divergent ncORF sets [20]. Consequently, published estimates of ncORF abundance span several orders of magnitude—ranging from thousands to millions [15-22]. To establish a standardized reference, the GENCODE consortium integrated data from seven distinct studies to produce a catalog of 7,264 human ncORFs (hereafter GENCODE ncORFs)[2]; however, the heterogeneity of sample sources and prediction algorithms likely introduced systematic bias. This catalog is also restricted to AUG-initiating ORFs, thereby overlooking those with near-cognate start codons. A later effort generated a high-resolution human translatome map and identified 7,767 ncORFs with a unified pipeline[22]. Nevertheless, this conservative annotation disproportionately under-represents coding sequence (CDS)-overlapping ncORFs. Indeed, later estimation suggests that between 10,500 to 22,500 ncORFs should exist in the human genome[18]. Furthermore, many ncORFs were reported from studies of cancer cells[1,13,23,24], where extensive transcriptome reprogramming alters the translational landscape[25,26]. While paired healthy tissues were also analyzed in these studies, the landscape of ncORFs translated under normal physiological conditions is not yet fully resolved.

While a limited subset of ncORFs has been shown to encode signaling molecules, cofactors, membrane proteins, or subunits of large protein complexes[1,27,28], functions of most ncORF-encoded proteins (ncEPs) are largely uncharacterized. Advances in high-throughput screen technologies have enabled the systematic interrogation of functional ncEPs[23,28,30-33]. Nevertheless, there is minimal concordance among hits from different studies[3]. Evolutionary analyses can offer insights into potential functionality of these translation products and mechanisms of origination[34-36], yet how ncORF translation has been remodeled to integrate into proteome since their evolutionary origins is still poorly understood. Consequently, the extent to which translated ncORFs encode functional proteins and the

evolutionary dynamics of their integration into the existing proteome are largely unresolved. Moreover, because most ncORF studies have focused on humans, it is unclear whether ncORFs in other species share similar sequence features and expression patterns.

To address these gaps, we generated a standardized annotation of translated ncORFs by uniformly reprocessing ~400 high-quality ribosome profiling libraries from normal mammalian tissues and cell types. This stringent approach yielded 11,623 human and 16,485 mouse ncORFs, consistently recovered across diverse samples and prediction strategies. Comparative and functional genomic analyses revealed that thousands of these ncORFs are under evolutionary constraint and exhibit distinct translation profiles. The resulting dataset provides a robust, comprehensive resource that will facilitate future investigations into the biological roles of ncORFs across cellular and organismal contexts.

Results

Annotation of ncORFs translated in normal mammalian cells

We developed a standardized pipeline to systematically annotate ncORFs translated in normal human and mouse cells (Fig. 1A). We first curated publicly available Ribo-Seq libraries, excluding those from pathological or genetically modified samples. Since both library size and the proportion of in-frame ribosome-protected fragments (RPFs) affect the sensitivity and accuracy of ncORF prediction[20], we filtered out libraries containing fewer than 5 million RPFs or with in-frame rates below 60%. After this quality control step, we retained 174 human and 209 mouse high-quality Ribo-Seq libraries, spanning a range of tissues and cell types (Fig. S1; Table S1). We predicted translated ORFs that begin with NUG (where N stands for any nucleotide) start codons and encode at least five amino acids using three tools—PRICE[37], RiboCode[38] and Ribo-TISH[39]—which we previously benchmarked for optimal performance[20]. After excluding annotated CDSs and their extension or truncation variants arising from alternative initiation sites, we obtained a preliminary list of ncORFs in each library.

To generate reliable ncORF annotations, we applied stringent filtering and integration criteria. We removed potential false positives caused by non-ribosomal contamination or translational noise based on metrics including Fragment Length Organization Similarity Score (FLOSS)[40], Ribosomal Release Score (RRS)[41,42] and the number of RPFs within an ORF by P-site. We then aggregated the remaining ORFs to identify those consistently detected across multiple methods and libraries in human and mouse datasets, respectively (Fig. 1A). In many cases, two ORFs predicted from different libraries or methods may share the same start or stop codon due to the alternative translation initiation or splicing, resulting in groups of overlapping ncORFs. For example, 11.1% (805) of GENCODE ncORFs overlap with at least one other ORF, forming 329 overlapping groups (Table S2). This overlap complicates the identification of reproducible ORFs, as ORFs within a group may represent distinct proteoforms of a protein. To address this issue, we collapsed each group of ncORFs sharing the same start or stop codon into a single cluster, and retained only those clusters supported by at least two independent methods and observed in more than one library. For each retained cluster, we selected a representative ORF by

prioritizing transcript annotation[43,44], start codon type, and ORF length to facilitate downstream analyses (Fig. 1A).

This approach yielded 12,469 translated ncORFs in humans and 16,960 in mice. However, manual inspection revealed a subset of spurious ncORFs that are not truncation or extension variants of annotated CDSs, but instead partially overlap with annotated CDSs from alternative transcript isoforms in frame (Figs. 1B & C). For instance, in gene *AGTPBP1*, the CDS of transcript *ENST00000357081* begins downstream of *ENST00000628899* CDS due to the inclusion of an alternative exon. As a result, the 5' UTR of *ENST00000357081* appears to contain a translated uORF (Fig. 1B), which overlaps in-frame with the CDS of *ENST00000628899* and may be mistakenly identified as a translated ncORF owing to active translation of the latter. A similar case is seen with the lncRNA ORF (lncORF) in *ENST00000462211*, which overlaps in-frame with the CDS of *ENST00000328767* from the *TMTC4* gene and may thus be erroneously identified as a translated ncORF (Fig. 1C). To avoid such artifacts, we implemented an additional filtering step to exclude these overlapping cases and left with 11,623 and 16,485 high-confidence ncORFs in humans and mice, respectively (Table S3).

Annotated ncORFs are supported by independent evidence

To assess whether the annotated ncORFs are supported by independent evidence, we compared them with a previously compiled catalog of ncORFs identified using mass spectrometry (MS)-based proteomic data[20]. For the 3,494 MS-supported ncORFs in humans and 873 in mice, 44.5% and 67.6%, respectively, were also predicted as translated ncORFs in this study (Fig. S2). We further evaluated our annotation against the GENCODE ncORFs[2], a widely used community resource. Of the 7,264 GENCODE ncORFs, 6,974 are located in fully annotated transcripts and were included in our analysis. Among them, 2,997 were reported by at least two independent studies (hereafter "phase 1"), while the remaining were only reported in a single study ("single")[2]. We found that 75.6% of phase 1 ncORFs were independently recovered in our annotation, significantly more than the single-study ncORFs (Fig. 1D; $P = 6.4\times10^{-307}$, Fisher's exact test).

A recent study conducted a comprehensive pan-proteome analysis to provide high-confidence peptide evidence for GENCODE ncORFs[45]. In this study, ncORFs were categorized into four tiers: tier 1 and 2 ncORFs had support from both MS and Ribo-Seq data; tier 3 had MS evidence only; and tier 4 had Ribo-Seq evidence only[29]. Notably, our annotation was significantly enriched for tier 1 or 2 ncORFs ($P = 2.0\times10^{-64}$, Fisher's exact test), with 446 and 661 of them detected, respectively (Fig. 1E). Combining MS-supported ncORFs from our previous compilation and those from GENCODE ncORFs, 2,088 (18.0%) human ncORFs identified in this study were supported by MS evidence. Despite this overlap, the majority (65.2%) of human ncORFs in our annotation are not included in either of the two catalogs. This highlights both the complexity of the non-canonical translatome and the critical role of tissue diversity in comprehensive ncORF annotation.

To further validate our findings, we manually curated ncORFs with known functions from the literature. We identified 17 ncORFs in our annotation that have been experimentally confirmed to be translated—either through reporter assays or antibody detection—and shown to produce functional proteins (Fig. 1F; Table S4). Notably, 16 of these validated ncORFs are from humans, and only 12 are included in the GENCODE catalog. This analysis further underscores the accuracy and functional relevance of our annotations. Together, these results indicate that our annotation pipeline generates a robust and reliable catalog of translated ncORFs in mammals.

ncORFs exhibit signatures of translation and encode putative proteins lacking known domains

We classified ORFs into categories based on community recommendations[2] and found that the distribution of ORF types closely aligns with previous estimates[18]. In both human and mouse, uORFs, upstream overlapping ORFs (uoORFs), and lncORFs are more prevalent than other types, whereas internal ORFs (iORFs), downstream overlapping ORFs (doORFs), and dORFs are relatively rare (Fig. 2A). Although most ncORFs are short, encoding fewer than 100 amino acids (Fig. 2B), their sequences show clear signatures of translation similar to CDSs. These include preferential usage of AUG start codons (Fig. S3A), enrichment toward 5' transcript ends (Fig. S3B), and reduced RNA secondary structure[46] (Fig. S3C) and optimized Kozak contexts[47,48] around start codons, especially in non-AUG ncORFs (Figs. S3D & S4). Despite these similarities, ncORFs differ markedly from CDSs in both codon and amino acid usage (Figs. S5A-B). This divergence is further supported by their lower tRNA adaptation index values and higher effective number of codons, indicating less optimized codon usage (Figs. S5C-D). Together, these findings show that ncORFs share core sequence and structural features with canonical CDSs, yet maintain distinct codon and amino acid usage profiles.

Although ncORFs can encode putative proteins, the functional significance of ncEPs remains poorly understood. To assess their potential functions, we searched for known protein domains within their sequences. Overall, only 1.29% (150) of human and 0.78% (129) of mouse ncEPs contained at least one known domain (Fig. 2C; Table S5), presumably due to their short lengths relative to canonical proteins. Consistently, domain-containing ncORFs are significantly longer than those without annotated domains (Fig. S6) and are predominantly classified as lncORFs (Fig. 2D). Unlike canonical proteins, which have relatively low intrinsically disordered region (IDR) content (median ± standard error: 14.6±0.28% in humans and 12.7±0.26% in mice), ncEPs exhibit significantly higher IDR proportions (Fig. 2E), with medians of 62.5±1.42% and 60.0±1.27%, respectively. These results indicate that most ncEPs lack structured domains and are instead dominated by IDRs.

Among the eight domains observed in at least five ncORFs, three are DNA-binding domains: zinc finger, Krüppel-associated box, and helix-turn-helix (Fig. 2F). We hypothesize that these domains might originate from transposable elements (TEs), which often encode DNA-binding proteins involved in transposition[49]. Indeed, domain-containing ncORFs were significantly enriched for TE overlap in

171 both humans and mice ($P = 5.8\times10^{-4}$ and 3.4×10^{-17}, respectively; Fisher's exact tests; Fig. 2G). Together,
172 these results suggest that only a subset of longer ncORFs have acquired modular domains, potentially
173 through TE-related mechanisms.
174
175 **Putative ncEPs are selectively constrained**
176 Given the scarcity of known domains in putative ncEPs, a key question is whether they are functional
177 in cells. If at least some of these ncEPs are not merely translational noise or byproducts of translation-
178 dependent functions, we would expect them to exhibit evolutionary signatures of selective constraints
179 similar to canonical CDSs. To test this, we leveraged the recent high-resolution genomic constraint
180 maps derived from both intra- and inter-species comparisons in humans [50,51]. First, we examined the
181 genomic non-coding constraint of haploinsufficient variation (Gnocchi), which quantifies selective
182 pressure by comparing observed versus expected variants across human genomes. A Gnocchi score
183 above zero indicates purifying selection[50]. Although Gnocchi scores of ncORFs are lower than those of
184 CDSs, they are significantly greater than zero (Fig. S7), suggesting that ncORF sequences are under
185 evolutionary constraint. A hallmark of functional coding regions is codon position-specific constraints,
186 but Gnocchi scores lack the resolution needed to assess such fine-scale features. Therefore, we next
187 analyzed the base-resolution conservation metric PhyloP[52] calculated from multiple alignments of
188 primate or mammalian genomes[51]. As expected, PhyloP scores in CDSs are substantially higher than
189 those in flanking UTRs and display strong three-nucleotide periodicity, with the third codon position
190 being less conserved than first and second (Fig. 3A). Although ncORFs (excluding those overlapping
191 annotated CDSs) do not show higher overall PhyloP than flanking regions, they also exhibit significant
192 three-nucleotide periodicity in both mammals (Fig. 3A) and primates (Fig. S8), suggesting that at least
193 a subset of ncORFs are subject to similar evolutionary constraints as CDSs.
194 Motivated by the above results, we next sought to identify individual ncORFs under selective
195 pressure. To this end, we determined their modes of origination[34,35] and evolutionary history through
196 comparative genomic analyses. Our analysis revealed that most ncORFs are evolutionarily young, with
197 63.0% (7,319) and 82.8% (13,508) ncORFs in humans and mice originating within the mammalian
198 lineage, respectively (Figs. 3B & S9). In line with previous studies[34,35], we estimate that at least 51.7%
199 of human and 50.8% of mouse ncORFs arise *de novo* (Table S6). We also observed that the number of
200 ncORFs originating at each ancestral node, when normalized by branch length, decreases with
201 increasing node-to-tip distance (Fig. 3C), reflecting dynamic turnover and reduced long-term retention
202 of ncORFs. To assess whether individual ncORFs are constrained for coding, we analyzed codon
203 substitution patterns within ncORFs since origination[34] with PhyloCSF[53]. PhyloCSF estimates the log-
204 likelihood ratio of a given alignment under coding versus non-coding models; positive values indicate
205 stronger similarity to conserved coding sequences. We found 13.8% (1,608) of human and 32.0% (5,281)
206 of mouse ncORFs have positive PhyloCSF scores (Fig. 3D), and 10.9% (1,264) of human and 22.6%
207 (3,721) of mouse ncORFs even have PhyloCSF exceeding 10 (Table S6), providing strong evidence

208 that these sequences may encode functional ncEPs.

209 Evolutionary dynamics can also provide insights into the function of ncORFs, as functionally
210 constrained ncORFs are less likely to be lost over time. To quantify the conservation of each ncORF
211 since its origination, we developed a local branch length score (BLS) (Fig. 4A), adapting the "global"
212 BLS metric previously used to assess uORF conservation across full phylogenies[48,54]. Unlike global
213 BLS, local BLS is designed to detect lineage-specific constraint, making it better suited for identifying
214 functional ncORFs that may be restricted to certain evolutionary branches. Using a local BLS threshold
215 of 0.9, we identified 16.3% (1,889) of human and 24.8% (4,087) of mouse ncORFs as exhibiting
216 lineage-specific conservation (Figs. 4B & S9). Notably, these ncORFs are significantly more likely to
217 show positive PhyloCSF scores (Fig. 4C), reflecting the effectiveness of local BLS. In total, we
218 identified 681 human and 1,622 mouse ncORFs that are both lineage-specifically conserved and show
219 evidence of coding potential, making them strong candidates for future functional validation. Together,
220 these findings suggest that a subset of ncORFs may encode functional proteins rather than translational
221 byproducts.

222

223 **Expression of ncORFs is shaped by their evolutionary dynamics**

224 Gene expression is a tightly regulated process, and non-functional products are unlikely to be robustly
225 expressed. To assess the expression of ncORFs, we examined their translation across diverse tissues
226 and cell lines (Table S7). On average, 71.9% of human and 48.5% of mouse ncORFs are translated with
227 reads per kilobase per million mapped reads (RPKM) ≥ 1, which is comparable to or slightly exceeds
228 the proportions observed for CDSs (Fig. S10). To investigate the influence of ncORF evolution on their
229 expression, we analyzed mean translation levels of ncORFs across different samples. We found that
230 ncORFs with higher local BLS tend to be more highly translated in both species (Fig. S11A), whereas
231 coding potential showed only a minor influence (Fig. S11B). To disentangle the effects of evolutionary
232 constraint and gene age, we stratified ncORFs by origination nodes and examined their translation levels
233 in relation to local BLS and PhyloCSF. Although ancient ncORFs are generally more highly translated,
234 those with higher local BLS scores consistently show elevated translation levels compared to their age-
235 matched counterparts (Figs. 5A & S12A). This suggests that lineage-specific conservation is associated
236 with enhanced and possibly optimized translation, potentially reflecting acquired functional roles.
237 Conversely, the relationship between coding potential and translation is more nuanced: young ncORFs
238 with positive PhyloCSF scores tend to be more highly translated, while the opposite trend is observed
239 in ancient ncORFs (Figs. 5B & S12B). These patterns point to complex interplays between evolutionary
240 constraint, coding potential, and translational output, likely reflecting divergent selective pressures
241 across different ncORF age groups.

242 While the above analyses revealed the overall trends in ncORF translation, they overlooked the
243 heterogeneity across tissues and cell types. We found that ncORF translation exhibits strong tissue
244 specificity (Fig. S13), which may stem from either transcriptional bias in ncORF-containing genes or

post-transcriptional regulation specific to ncORFs. To disentangle these factors, we examined RNA levels of ncORF-containing genes across different tissues[55,56]. Although transcriptional enrichment in testis was evident in both humans and mice (Fig. S14), testis-biased translation was observed only in mice (Fig. S13). Moreover, ncORF translation displayed significantly higher tissue specificity than the transcription of their host genes in both species (Fig. 5C), indicating a substantial post-transcriptional component to their regulation. We next assessed how evolutionary characteristics shape tissue specificity. Ancient ncORFs tend to have lower tissue specificity than younger ones, suggesting they are more broadly translated (Figs. 5D & S12C). Intriguingly, coding potential exhibits opposite effects depending on evolutionary age: young ncORFs with higher coding potential are more broadly expressed, whereas ancient ones show increased tissue specificity (Figs. 5E & S12D). These patterns may help to explain the lower average translation levels observed for ancient ncORFs across tissues. A similar trend was also evident for ncORFs with high local constraint scores in mice (Fig. S12C). Collectively, these results support a model in which ncORFs initially evolve widespread expression to establish interactions and avoid loss[57], but may later become functionally specialized, resulting in more restricted expression.

Extensive co-translation between ncORFs and canonical CDSs

Given our earlier observation that many ncEPs lack modular domains and may act via interactions with canonical proteins, we next explored the landscape of co-translation between ncORFs and CDSs across different tissues or cell types as we expect that interacting proteins tend to be translated simultaneously spatiotemporally. Using weighted gene co-expression network analysis (WGCNA)[58], we identified 61,513 human and 55,449 mouse ncORF-CDS co-translated pairs. As expected, ncORFs in mRNAs tend to co-translate with the main CDS of the same gene, even after excluding CDS-overlapping ones (Fig. S15), consistent with previous experimental findings[28]. This co-translation forms a highly modular bipartite network, in which one CDS may be linked to multiple ncORFs and vice versa (Fig. 6A-B). Network analysis revealed that hub CDS nodes—those with the most connections—in the largest modules are significantly enriched for functional gene categories (Fig. 6C-D). For instance, the largest module in humans is associated with chromatin-related proteins, while the second largest module in humans and the largest one in mice are linked to extracellular matrix organization. Notably, ancient ncORFs (those originating before the last common ancestor of mammals) are significantly more likely to co-translate with CDSs than younger ones (Fig. 6E), potentially reflecting a greater likelihood of acquiring functional interactions over evolutionary time. In summary, our analyses revealed that evolutionary dynamics of ncORFs have widespread impacts on their translation and potential function.

Discussion

Reliable annotation of translated ncORFs is critical for understanding their functional roles and evolutionary significance. In this study, we developed a standardized pipeline for the annotation of

translated ncORFs and applied it to both humans and mice due to the extensive publicly available Ribo-Seq datasets. Compared to previous efforts, our annotation framework offers several key improvements. First, we selected only high-quality libraries with sufficient read coverage and acceptable in-frame RPF rates. Our earlier work demonstrated that both library size and in-frame rates impact the reproducibility and accuracy of ncORF predictions[20]. This step helps mitigate false annotations arising from suboptimal data quality. Second, although many previously characterized functional ncEPs are associated with cancer-related ncORFs[1], ncORFs may also have important functions under physiological conditions. Importantly, such ncORFs are more likely to be subject to evolutionary constraints. Therefore, we restricted our analysis to normal cells and tissues, allowing us to identify more biologically relevant and conserved ncORFs. Third, given the variable performance across ncORF detection methods and the low reproducibility of predictions between biological replicates[20], we implemented stringent reproducibility criteria. Specifically, we retained only ncORFs detected by multiple methods and across independent datasets, enhancing the robustness of our final annotation. Finally, we applied a suite of well-validated filtering metrics from prior studies[40-42] to minimize the inclusion of false positives, including those arising from translational noise[59,60] or non-ribosomal contamination. As a result, our annotated ncORFs show significant enrichment for GENCODE ncORFs, especially those with MS evidence or reproducible detection across independent studies. These features collectively underscore the reliability and utility of our annotation for future functional and evolutionary studies of non-canonical translation.

From the perspective of new gene evolution, ncORFs represent a transitional stage between non-coding DNA/RNA and protein-coding genes[61,62]. A major challenge in reclassifying ncORFs as bona fide coding genes lies in determining whether the putative proteins they encode are functionally relevant. Our analysis of ncEPs revealed that most lack recognizable protein domains and are enriched for IDRs. Therefore, we propose that many ncORFs may function in a non-autonomous manner by interacting with other proteins to exert their effects. This hypothesis aligns with prior studies showing physical interactions between ncEPs and known proteins[28,30,35]. Supporting this view, our WGCNA analysis uncovered widespread co-translation between ncORFs and canonical CDSs, suggesting potential interaction partners and functional contexts.

We also assessed whether ncORFs are subject to evolutionary constraints consistent with functional protein coding. Using both population-level and cross-species analyses, we found that many ncORFs are under purifying selection, and their sequence conservation patterns often exhibit base-level features reminiscent of canonical CDSs—albeit to a lesser degree. Furthermore, we reconstructed the evolutionary trajectories of thousands of ncORFs in both humans and mice and observed sustained coding potential since their origination. Complementing these findings, we identified a subset of ncORFs that preserve intact ORF structures across most descendant species, suggesting ongoing purifying selection against disabling mutations. These lineage-specifically conserved and potentially coding ncORFs likely contribute to clade-specific functional innovation and represent compelling candidates for future functional characterization.

We further explored how evolutionary history shapes ncORF translation across tissues or cell types. Our results indicate that ancient ncORFs are more broadly and highly translated and have established more extensive co-expression with canonical CDSs. Moreover, when comparing ncORFs of similar age, those that are lineage-specifically constrained consistently exhibit higher translation levels, reinforcing their likely functional importance. Interestingly, we found that young ncORFs with strong evolutionary constraints tend to have lower tissue specificity in their translation, potentially reflecting a phase of widespread expression that facilitates functional recruitment. In contrast, older ncORFs with positive coding potential tend to display increased tissue specificity, implying functional specialization over evolutionary time. Collectively, these findings support a model in which ncORFs evolve from broadly expressed, weakly functional elements into specialized, conserved effectors—though further empirical work is needed to validate this hypothesis.

In conclusion, we provide a comprehensive annotation of translated ncORFs in humans and mice, offering a valuable resource for functional and evolutionary genomics. Our integrated analysis of sequence evolution and translational landscape sheds light on the evolutionary trajectory and functional integration of ncORFs. The consistency of these patterns in both species suggests that our findings may generalize to other mammals. However, realizing the full biological significance of ncORFs, particularly lineage-specific ones, will require experimental validation. Recent advances in high-throughput screening technologies[19,30,33,63] offer a promising path forward. Lastly, although our study focused on humans and mice due to the availability of high-quality Ribo-Seq data, we anticipate that our annotation will serve as a training resource for machine learning models aimed at predicting translated ncORFs in non-model organisms, thus broadening our understanding of genome coding potential across species.

Methods

Quality control and preprocessing of Ribo-Seq libraries

Ribo-Seq libraries from normal human or mouse samples without genetic modifications or perturbations (Table S7) were downloaded from the European Nucleotide Archive (ENA) or the Short Read Archive (SRA). For ncORF annotation, libraries containing fewer than five million reads were excluded. Libraries derived from cancer tissues or cell lines were also removed based on sample metadata or the associated publications. Next, adapter sequences and any random nucleotide additions were trimmed using Cutadapt (v3.7)[64] and reads shorter than 18 nucleotides were discarded. Remaining reads were aligned to the human or mouse reference genome (GRCh38 or GRCm39, ENSEMBL[65] release 107) using the STAR aligner (v2.7.10a)[66]. To assess library quality, the proportion of in-frame ribosome-protected fragment (RPF) reads was calculated using the PSite package[67]. Libraries with ≥60% in-frame RPFs were classified as high quality. Only samples containing at least two high-quality libraries were retained for ncORF annotation (Table S1). For the expression analyses, all the downloaded Ribo-Seq

libraries were used to cover more samples.

ncORF annotation

For each Ribo-Seq library, translated ORFs initiating with AUG, CUG, GUG, or UUG and encoding at least five amino acids were predicted using PRICE[37], RiboCode[38], and Ribo-TISH[39], as described previously[20]. To define novel ORFs, annotated CDSs and their truncation or extension variants (i.e., ORFs with the same start or stop position as annotated CDSs) were excluded. To eliminate likely false positives resulting from non-ribosomal contamination or stochastic molecular errors, we calculated RRS[41,42] and FLOSS[40] of each ncORF. RRS measures the drop in RPF coverage after stop codon—a key signature of active translation beyond three-nucleotide periodicity[41,42], whereas FLOSS assesses whether the RPF length distribution resembles that of canonical CDSs, helping to distinguish authentic ORFs from non-ribosomal signals[40]. In each library, uniquely mapped RPFs were assigned to the corresponding P-site, and genome-wide P-site coverage was computed with the PSite package. Similar to previous studies[41,42], RRS was calculated as the sum of coverage across the five codons preceding the stop codon divided by the sum across the five trinucleotides following the stop codon. FLOSS was calculated by first deriving a reference RPF length distribution vector (P_{ref}) using all RPFs uniquely mapped to annotated CDSs. For each ORF (ncORF or CDS), a read length frequency vector (P_{ORF}) was computed, and FLOSS was calculated as $\sum\left|P_{ref} - P_{ORF}\right|/2$. The empirical upper bound for acceptable FLOSS was set using Tukey's method (i.e., the third quartile + 1.5 × inter-quartile range of FLOSS values across all CDSs)[40]. ncORFs with fewer than 10 P-site-mapped RPFs, RRS ≤ 1, or FLOSS values exceeding the empirical upper bound were filtered out.

Integration of ncORF prediction across different libraries of the same species was nontrivial due to extensive overlap among ncORFs in genomic coordinates. To address this issue, we used a graph-based clustering approach. We created a graph where two ORF vertices were connected if they share the same start or stop codon. Then, each set of connected ncORFs in the graph represents a cluster of overlapping ncORFs. To ensure reproducibility, only clusters identified by ≥2 methods in ≥2 libraries were retained, yielding 13,071 clusters in humans and 17,674 clusters in mice. To ensure compatibility with the latest reference gene annotations (ENSEMBL release 111), we removed any ncORFs that were newly classified as annotated CDSs. A manual inspection of RPF signals using the GWIPS-viz Ribo-Seq track[68] in the UCSC Genome Browser[69] revealed additional spurious ncORFs overlapping in-frame with CDSs from other transcripts. These were likely misidentified due to shared translation signals and were conservatively excluded using custom scripts, leaving 11,623 clusters in humans and 16,485 in mice.

To facilitate downstream analyses, a representative ncORF was selected for each cluster using a two-step strategy. First, a representative transcript was selected by prioritizing those with matched annotation from NCBI and EMBL-EBI (MANE)[43] (for humans) or APPRIS principal[70]; otherwise, the

longest transcript was chosen. Then, among ncORFs within the representative transcript, a single ncORF was selected based on start codon hierarchy (AUG > CUG/GUG > UUG) following empirical evidence[28,37]. If multiple ncORFs shared the same preferred start codon, the longer one was chosen.

For validation, our ncORFs were compared with previously annotated GENCODE ncORFs[2] and those with MS evidence compiled previously[20]. Tier annotations of GENCODE ncORFs were obtained from a recent study[29]. Known functional ncORFs and their genomic coordinates were manually curated from published literature (Table S4). To account for possible proteoforms arising from alternative initiation and splicing, we considered an ncORF to be recovered if either its start or stop codon was identical to any ncORF in our annotation.

ncORF sequence analyses

The secondary structure surrounding each ORF (ncORF or CDS) start codon was predicted with RNAfold[71] on a 150 nt window extracted from the transcript in which the ncORF resides starting from the 30th nucleotide upstream of the start codon. For each position within this window, the overall pairing probability was calculated by dividing the number of ORFs with a base-paired residue at that position by the total number of ORFs analyzed. The tRNA adaptation index and effective number of codons for ncORFs and CDSs were calculated using the "cubar" R package[72]. tRNA gene annotations in humans and mice were obtained from GtRNAdb (release 22)[73].

Putative ncEPs analyses

Known domains within ncEPs were identified using InterProScan (v5.64-96.0)[74] with default parameters. Repetitive sequence annotations were downloaded from the UCSC Table Browser. BEDTools (v2.31.1)[75] was used to identify TE-overlapping ncORFs. IDRs were predicted with IUPred3[76] with analysis type set to "short disorders" and smoothing disabled. For each ORF, residues with disorder tendency score > 0.5 were considered disordered, and the IDR fraction was calculated as the proportion of disordered residues relative to the ORF length.

Gnocchi Score and PhyloP of ncORFs and CDSs

Genome-wide Gnocchi scores computed using 1 kb sliding windows (with 100bp step size) were downloaded from the gnomAD database[50]. For each base pair, the Gnocchi score was defined as the average across the ten overlapping 1kb windows that covered that position using BEDTools. The final Gnocchi score for each ORF (ncORF or CDS) was obtained by averaging the scores of all base pairs within the ORF.

Base-wise PhyloP scores computed across 441 mammals or 239 primates[51] were downloaded from the UCSC Genome Browser. For each ncORF or CDS, PhyloP values were extracted for a ±30 bp window surrounding the start and stop codons using custom scripts. These values were then averaged over different ORFs to generate metagene profiles for visualization. To evaluate three-nucleotide

429 periodicity, the metagene profiles were subjected to autocorrelation analysis using the "ac.test" function
430 from the "testcorr" R package[77]. Statistical significance was assessed using the robust $\tilde{t}$ statistics.
431
432 **ncORF origination node and mode**
433 Whole genome alignments and corresponding species trees were downloaded from the UCSC Genome
434 Browser (GRCh38 100-way for humans and GRCm39 35-way for mice). The origination node and
435 mode for each ncORF were inferred following previous approaches[34,35]. For each ORF, the sequence
436 from the reference genome and its orthologous regions in other species were extracted. Orthologous
437 sequences covering less than 50% of the ncORF length relative to the reference species were excluded.
438 The remaining sequences were realigned with MAFFT (v7.520)[78] with default parameters. The
439 corresponding gene tree was derived by pruning the species tree using Gotree (v0.4.3)[79] with default
440 settings. Ancestral sequence reconstruction was performed using FastML (v3.11)[80] with parameters "--
441 seqType nuc --SubMatrix HKY --OptimizeBL no --indelReconstruction ML". An ORF structure was
442 considered intact in an orthologous or ancestral sequence if one of the first three codons was a start
443 codon and at least 70% of the 5' region of the reference ncORF was free of in-frame stop codons. The
444 origination node was defined as the most ancient ancestral node that retained an intact ORF structure.
445 An ncORF was classified as *de novo* if the origination node had an ancestor covering at least 50% of
446 the ncORF sequence but lacking an intact ncORF structure. Otherwise, the origination mode was
447 classified as uncertain. The distance from an ancestral node to the reference species (tip node) was
448 calculated by summing branch lengths along the connecting path using the ape R package (v5.8)[81].
449
450 **ncORF BLS and PhyloCSF**
451 For each ncORF, global BLS was calculated as the ratio of the total branch length of the subtree
452 connecting all leaves with intact ORF structures to the total branch length of the full species tree as in
453 our previous study[48] with custom scripts. Local BLS was calculated similarly, but the denominator was
454 replaced by the total branch length of the subtree defined by the origination node and all of its
455 descendant nodes (including leaves). To evaluate coding potential, the alignment of all species
456 descending from the origination node was converted into Multiple Alignment Format after removing
457 the stop codon. PhyloCSF scores were then computed using the "score-msa" module of PhyloCSF++[82].
458
459 **ncORF expression analysis**
460 To quantify translation levels of ncORFs and CDSs in Ribo-Seq libraries, we assigned uniquely mapped
461 reads to corresponding P-site positions with the PSite package. The read count for each ORF was
462 calculated as the total number of RPFs whose P-sites fell within the ORF. To reduce bias caused by RPF
463 enrichment at ORF termini, reads mapping to start or stop codons were excluded. For CDSs, only the
464 count of the representative transcript of each gene as defined above was used for downstream analyses.
465 For samples with multiple libraries, read counts were aggregated prior to normalization. Sample-

466 specific size factors were estimated using CDS counts and applied to normalize both ncORF and CDS
467 counts across samples using DESeq2[83]. RPKM for an ORF was calculated as normalized read counts /
468 ORF length (nt) / library size × 10^9, where library size was the median of total read counts across
469 samples to ensure cross-sample comparability. An ORF (ncORF or CDS) was considered translated if
470 its RPKM was ≥ 1. To evaluate tissue specificity of ncORF translation, the normalized RPF count X_k
471 of an ORF in sample k was log-transformed as $x_k = log(X_k + 1)$. Then, tissue specificity index[84] was
472 calculated as $\tau = \sum_k^n (1 - \tilde{x}_k)/(n-1)$, where $\tilde{x}_k = x_k / \max_{1 \le j \le n} x_j$ and n is the total number of samples.
473 To quantify RNA levels, raw reads of deep transcriptome profiling across different human or mouse
474 tissues from previous studies[55,56] were downloaded from SRA. Gene expression levels (transcript per
475 million, TPM) were estimated using salmon (v1.10.3)[85] with parameters "--seqBias --gcBias --posBias
476 -l A".
477 WGCNA analysis[58] of ncORF and CDS translation was performed using the PyWGCNA
478 package (v2.0.5)[86] with default settings. Only ORFs with normalized RPF counts ≥ 10 in more than half
479 of the samples were included. The soft threshold was determined automatically by PyWGCNA. Due to
480 differences in soft thresholds, two ORFs were considered cotranslated if their topological overlap > 0.1
481 (human) or > 0.01 (mouse).[58] To test whether co-translation is enriched between ncORFs and CDSs
482 from the same transcript, gene identities of CDSs were randomly permuted among all co-translated
483 ncORF–CDS pairs. This procedure was repeated 1,000 times, and the empirical *P* value was calculated
484 as (m + 1) / 1,000, where m is the number of permutations in which the number of same-gene pairs was
485 greater than or equal to the observed count. The bipartite network of ncORF-CDS co-translation was
486 clustered using the Leiden algorithm[87] implemented in igraph (v2.1.3)[88] by optimizing modularity with
487 a resolution of 0.2. The top 20% of nodes by betweenness centrality were designated as hub nodes.
488 Gene ontology analysis of hub genes in the largest modules was conducted using ClusterProfiler
489 (v4.12)[89].
490
491 **Code availability**
492 All analyses were primarily conducted using R software (v4.3). Unless otherwise stated, statistical tests
493 are two-sided. The code is available at https://github.com/gxelab/ncorf_mammals and custom scripts
494 can be found at https://github.com/gxelab/scripts.
495
496 **Data availability**
497 Ribo-Seq libraries for ncORF annotation were obtained from the ENA or SRA, with accession codes
498 listed in Table S1. Libraries used for ncORF and CDS translation quantification were listed in Table S7.
499 RNA-Seq libraries for gene expression profiling across different human or mouse tissues were from
500 previous studies[55,56] and are available with ENA accession numbers E-MTAB-2836 and E-MTAB-
501 10276, respectively. Whole genome alignment across vertebrates, annotation of genomic repetitive

elements, and base-wise PhyloP in primates and mammals[51] were downloaded from the UCSC Genome Browser[69]. Gnocchi scores were downloaded from gnomAD[50]. All the other data were presented in the manuscript or supplementary tables and are available from the corresponding author upon reasonable request.

Competing interests

The authors declare that they have no competing interests.

Acknowledgments

We thank Dr. Chuan Yan and all the Zhang lab members for helpful discussion. This study was supported by the National Natural Science Foundation of China (32200433) and the Fundamental Research Funds for the Central Universities (LZUJBKY-2022-2). We thank the Supercomputing Center of Lanzhou University for providing computational resources.

References

1. Wright, B.W., Yi, Z., Weissman, J.S., and Chen, J. (2021). The dark proteome: translation from noncanonical open reading frames. Trends in Cell Biology. 10.1016/j.tcb.2021.10.010.
2. Mudge, J.M., Ruiz-Orera, J., Prensner, J.R., Brunet, M.A., Calvet, F., Jungreis, I., Gonzalez, J.M., Magrane, M., Martinez, T.F., Schulz, J.F., et al. (2022). Standardized annotation of translated open reading frames. Nature Biotechnology *40*, 994-999. 10.1038/s41587-022-01369-0.
3. Azam, S., Yang, F., and Wu, X. (2025). Finding functional microproteins. Trends Genet *41*, 107-118. 10.1016/j.tig.2024.12.001.
4. Baena-Angulo, C., Platero, A.I., and Couso, J.P. (2025). Cis to trans: small ORF functions emerging through evolution. Trends Genet *41*, 119-131. 10.1016/j.tig.2024.10.012.
5. Hofman, D.A., Prensner, J.R., and van Heesch, S. (2025). Microproteins in cancer: identification, biological functions, and clinical implications. Trends Genet *41*, 146-161. 10.1016/j.tig.2024.09.002.
6. Orr, M.W., Mao, Y., Storz, G., and Qian, S.B. (2020). Alternative ORFs and small ORFs: shedding light on the dark proteome. Nucleic Acids Research *48*, 1029-1042. 10.1093/nar/gkz734.
7. Lu, S., Zhang, J., Lian, X., Sun, L., Meng, K., Chen, Y., Sun, Z., Yin, X., Li, Y., Zhao, J., et al. (2019). A hidden human proteome encoded by 'non-coding' genes. Nucleic Acids Res *47*, 8111-8125. 10.1093/nar/gkz646.
8. Ingolia, N.T., Ghaemmaghami, S., Newman, J.R., and Weissman, J.S. (2009). Genome-wide analysis in vivo of translation with nucleotide resolution using ribosome profiling. Science *324*, 218-223. 10.1126/science.1168978.
9. Mao, Y., Jia, L., Dong, L., Shu, X.E., and Qian, S.B. (2023). Start codon-associated ribosomal frameshifting mediates nutrient stress adaptation. Nature Structural & Molecular Biology *30*, 1816-1825. 10.1038/s41594-023-01119-z.
10. Ferguson, L., Upton, H.E., Pimentel, S.C., Mok, A., Lareau, L.F., Collins, K., and Ingolia, N.T. (2023). Streamlined and sensitive mono- and di-ribosome profiling in yeast and human cells. Nature Methods *20*, 1704-1715. 10.1038/s41592-023-02028-1.
11. Wang, Y., Zhang, H., and Lu, J. (2020). Recent advances in ribosome profiling for deciphering translational regulation. Methods *176*, 46-54. 10.1016/j.ymeth.2019.05.011.
12. Cao, X., Sun, S., and Xing, J. (2024). A Massive Proteogenomic Screen Identifies Thousands of Novel Peptides From the Human "Dark" Proteome. Molecular & Cellular Proteomics *23*,

100719. 10.1016/j.mcpro.2024.100719.

13. Ouspenskaia, T., Law, T., Clauser, K.R., Klaeger, S., Sarkizova, S., Aguet, F., Li, B., Christian, E., Knisbacher, B.A., Le, P.M., et al. (2021). Unannotated proteins expand the MHC-I-restricted immunopeptidome in cancer. Nature Biotechnology *40*, 209-217. 10.1038/s41587-021-01021-3.

14. Wu, Q., Wright, M., Gogol, M.M., Bradford, W.D., Zhang, N., and Bazzini, A.A. (2020). Translation of small downstream ORFs enhances translation of canonical main open reading frames. EMBO Journal *39*, e104763. 10.15252/embj.2020104763.

15. Li, Y., Zhou, H., Chen, X., Zheng, Y., Kang, Q., Hao, D., Zhang, L., Song, T., Luo, H., Hao, Y., et al. (2021). SmProt: A Reliable Repository with Comprehensive Annotation of Small Proteins Identified from Ribosome Profiling. Genomics, Proteomics & Bioinformatics *19*, 602-610. 10.1016/j.gpb.2021.09.002.

16. Leblanc, S., Yala, F., Provencher, N., Lucier, J.F., Levesque, M., Lapointe, X., Jacques, J.F., Fournier, I., Salzet, M., Ouangraoua, A., et al. (2024). OpenProt 2.0 builds a path to the functional characterization of alternative proteins. Nucleic Acids Research *52*, D522-d528. 10.1093/nar/gkad1050.

17. Yang, H., Li, Q., Stroup, E.K., Wang, S., and Ji, Z. (2024). Widespread stable noncanonical peptides identified by integrated analyses of ribosome profiling and ORF features. Nat Commun *15*, 1932. 10.1038/s41467-024-46240-9.

18. Prensner, J.R., Abelin, J.G., Kok, L.W., Clauser, K.R., Mudge, J.M., Ruiz-Orera, J., Bassani-Sternberg, M., Moritz, R.L., Deutsch, E.W., and van Heesch, S. (2023). What Can Ribo-Seq, Immunopeptidomics, and Proteomics Tell Us About the Noncanonical Proteome? Molecular & Cellular Proteomics *22*, 100631. 10.1016/j.mcpro.2023.100631.

19. Valdivia-Francia, F., and Sendoel, A. (2024). No country for old methods: New tools for studying microproteins. iScience *27*, 108972. 10.1016/j.isci.2024.108972.

20. Lei, T., Chang, Y., Yao, C., and Zhang, H. (2023). A systematic evaluation of computational methods for predicting translated non-canonical ORFs from ribosome profiling data. Journal of Genetics and Genomics *51*, 105-108. 10.1016/j.jgg.2023.08.010.

21. Olexiouk, V., Crappé, J., Verbruggen, S., Verhegen, K., Martens, L., and Menschaert, G. (2016). sORFs.org: a repository of small ORFs identified by ribosome profiling. Nucleic Acids Research *44*, D324-D329. 10.1093/nar/gkv1175.

22. Chothani, S.P., Adami, E., Widjaja, A.A., Langley, S.R., Viswanathan, S., Pua, C.J., Zhihao, N.T., Harmston, N., D'Agostino, G., Whiffin, N., et al. (2022). A high-resolution map of human RNA translation. Molecular Cell *82*, 2885-2899.e2888. 10.1016/j.molcel.2022.06.023.

23. Prensner, J.R., Enache, O.M., Luria, V., Krug, K., Clauser, K.R., Dempster, J.M., Karger, A., Wang, L., Stumbraite, K., Wang, V.M., et al. (2021). Noncanonical open reading frames encode functional proteins essential for cancer cell survival. Nature Biotechnology *39*, 697-704. 10.1038/s41587-020-00806-2.

24. Camarena, M.E., Theunissen, P., Ruiz, M., Ruiz-Orera, J., Calvo-Serra, B., Castelo, R., Castro, C., Sarobe, P., Fortes, P., Perera-Bel, J., and Albà, M.M. (2024). Microproteins encoded by noncanonical ORFs are a major source of tumor-specific antigens in a liver cancer patient meta-cohort. Sci Adv *10*, eadn3628. 10.1126/sciadv.adn3628.

25. Sendoel, A., Dunn, J.G., Rodriguez, E.H., Naik, S., Gomez, N.C., Hurwitz, B., Levorse, J., Dill, B.D., Schramek, D., Molina, H., et al. (2017). Translation from unconventional 5' start sites drives tumour initiation. Nature *541*, 494-499. 10.1038/nature21036.

26. Robichaud, N., Sonenberg, N., Ruggero, D., and Schneider, R.J. (2019). Translational Control in Cancer. Cold Spring Harb Perspect Biol *11*. 10.1101/cshperspect.a032896.

27. Malekos, E., and Carpenter, S. (2022). Short open reading frame genes in innate immunity: from discovery to characterization. Trends Immunol *43*, 741-756. 10.1016/j.it.2022.07.005.

28. Chen, J., Brunner, A.D., Cogan, J.Z., Nunez, J.K., Fields, A.P., Adamson, B., Itzhak, D.N., Li, J.Y., Mann, M., Leonetti, M.D., and Weissman, J.S. (2020). Pervasive functional translation of noncanonical human open reading frames. Science *367*, 1140-1146. 10.1126/science.aay0262.

29. Deutsch, E.W., Kok, L.W., Mudge, J.M., Ruiz-Orera, J., Fierro-Monti, I., Sun, Z., Abelin, J.G., Alba, M.M., Aspden, J.L., Bazzini, A.A., et al. (2024). High-quality peptide evidence for annotating non-canonical open reading frames as human proteins. bioRxiv.

10.1101/2024.09.09.612016.
30. Zheng, C., Wei, Y., Zhang, P., Lin, K., He, D., Teng, H., Manyam, G., Zhang, Z., Liu, W., Lee, H.R.L., et al. (2023). CRISPR-Cas9-based functional interrogation of unconventional translatome reveals human cancer dependency on cryptic non-canonical open reading frames. Nature Structural & Molecular Biology *30*, 1878-1892. 10.1038/s41594-023-01117-1.
31. Zheng, C., Wei, Y., Zhang, P., Xu, L., Zhang, Z., Lin, K., Hou, J., Lv, X., Ding, Y., Chiu, Y., et al. (2023). CRISPR/Cas9 screen uncovers functional translation of cryptic lncRNA-encoded open reading frames in human cancer. J Clin Invest *133*. 10.1172/jci159940.
32. Schlesinger, D., Dirks, C., Luzon, C.N., Lafranchi, L., Eirich, J., and Elsässer, S.J. (2023). A large-scale sORF screen identifies putative microproteins and provides insights into their interaction partners, localisation and function. bioRxiv, 2023.2006.2013.544808. 10.1101/2023.06.13.544808.
33. Hofman, D.A., Ruiz-Orera, J., Yannuzzi, I., Murugesan, R., Brown, A., Clauser, K.R., Condurat, A.L., van Dinter, J.T., Engels, S.A.G., Goodale, A., et al. (2024). Translation of non-canonical open reading frames as a cancer cell survival mechanism in childhood medulloblastoma. Molecular Cell *84*, 261-276.e218. 10.1016/j.molcel.2023.12.003.
34. Vakirlis, N., Vance, Z., Duggan, K.M., and McLysaght, A. (2022). De novo birth of functional microproteins in the human lineage. Cell Rep *41*, 111808. 10.1016/j.celrep.2022.111808.
35. Sandmann, C.L., Schulz, J.F., Ruiz-Orera, J., Kirchner, M., Ziehm, M., Adami, E., Marczenke, M., Christ, A., Liebe, N., Greiner, J., et al. (2023). Evolutionary origins and interactomes of human, young microproteins and small peptides translated from short open reading frames. Mol Cell *83*, 994-1011.e1018. 10.1016/j.molcel.2023.01.023.
36. Wacholder, A., Parikh, S.B., Coelho, N.C., Acar, O., Houghton, C., Chou, L., and Carvunis, A.R. (2023). A vast evolutionarily transient translatome contributes to phenotype and fitness. Cell Syst. 10.1016/j.cels.2023.04.002.
37. Erhard, F., Halenius, A., Zimmermann, C., L'Hernault, A., Kowalewski, D.J., Weekes, M.P., Stevanovic, S., Zimmer, R., and Dolken, L. (2018). Improved Ribo-seq enables identification of cryptic translation events. Nat Methods *15*, 363-366. 10.1038/nmeth.4631.
38. Xiao, Z., Huang, R., Xing, X., Chen, Y., Deng, H., and Yang, X. (2018). De novo annotation and characterization of the translatome with ribosome profiling data. Nucleic Acids Res *46*, e61. 10.1093/nar/gky179.
39. Zhang, P., He, D., Xu, Y., Hou, J., Pan, B.F., Wang, Y., Liu, T., Davis, C.M., Ehli, E.A., Tan, L., et al. (2017). Genome-wide identification and differential analysis of translational initiation. Nat Commun *8*, 1749. 10.1038/s41467-017-01981-8.
40. Ingolia, N.T., Brar, G.A., Stern-Ginossar, N., Harris, M.S., Talhouarne, G.J., Jackson, S.E., Wills, M.R., and Weissman, J.S. (2014). Ribosome profiling reveals pervasive translation outside of annotated protein-coding genes. Cell Rep *8*, 1365-1379. 10.1016/j.celrep.2014.07.045.
41. Chew, G.L., Pauli, A., Rinn, J.L., Regev, A., Schier, A.F., and Valen, E. (2013). Ribosome profiling reveals resemblance between long non-coding RNAs and 5' leaders of coding RNAs. Development *140*, 2828-2834. 10.1242/dev.098343.
42. Guttman, M., Russell, P., Ingolia, N.T., Weissman, J.S., and Lander, E.S. (2013). Ribosome profiling provides evidence that large noncoding RNAs do not encode proteins. Cell *154*, 240-251. 10.1016/j.cell.2013.06.009.
43. Morales, J., Pujar, S., Loveland, J.E., Astashyn, A., Bennett, R., Berry, A., Cox, E., Davidson, C., Ermolaeva, O., Farrell, C.M., et al. (2022). A joint NCBI and EMBL-EBI transcript set for clinical genomics and research. Nature *604*, 310-315. 10.1038/s41586-022-04558-8.
44. Pozo, F., Rodriguez, J.M., Martínez Gómez, L., Vázquez, J., and Tress, M.L. (2022). APPRIS principal isoforms and MANE Select transcripts define reference splice variants. Bioinformatics *38*, ii89-ii94. 10.1093/bioinformatics/btac473.
45. Chothani, S., Ruiz-Orera, J., Tierney, J.A.S., Clauwaert, J., Deutsch, E.W., Alba, M.M., Aspden, J.L., Baranov, P.V., Bazzini, A.A., Bruford, E.A., et al. (2025). An expanded reference catalog of translated open reading frames for biomedical research. bioRxiv. 10.1101/2025.07.03.662928.
46. Shabalina, S.A., Spiridonov, N.A., and Kashina, A. (2013). Sounds of silence: synonymous

nucleotides as a key to biological regulation and complexity. Nucleic Acids Res *41*, 2073-2094. 10.1093/nar/gks1205.

47. Hernández, G., Osnaya, V.G., and Pérez-Martínez, X. (2019). Conservation and Variability of the AUG Initiation Codon Context in Eukaryotes. Trends Biochem Sci *44*, 1009-1021. 10.1016/j.tibs.2019.07.001.
48. Zhang, H., Wang, Y., Wu, X., Tang, X., Wu, C., and Lu, J. (2021). Determinants of genome-wide distribution and evolution of uORFs in eukaryotes. Nature Communications *12*, 1076. 10.1038/s41467-021-21394-y.
49. Wells, J.N., and Feschotte, C. (2020). A Field Guide to Eukaryotic Transposable Elements. Annu Rev Genet *54*, 539-561. 10.1146/annurev-genet-040620-022145.
50. Chen, S., Francioli, L.C., Goodrich, J.K., Collins, R.L., Kanai, M., Wang, Q., Alföldi, J., Watts, N.A., Vittal, C., Gauthier, L.D., et al. (2024). A genomic mutational constraint map using variation in 76,156 human genomes. Nature *625*, 92-100. 10.1038/s41586-023-06045-0.
51. Kuderna, L.F.K., Ulirsch, J.C., Rashid, S., Ameen, M., Sundaram, L., Hickey, G., Cox, A.J., Gao, H., Kumar, A., Aguet, F., et al. (2024). Identification of constrained sequence elements across 239 primate genomes. Nature *625*, 735-742. 10.1038/s41586-023-06798-8.
52. Pollard, K.S., Hubisz, M.J., Rosenbloom, K.R., and Siepel, A. (2010). Detection of nonneutral substitution rates on mammalian phylogenies. Genome Res *20*, 110-121. 10.1101/gr.097857.109.
53. Lin, M.F., Jungreis, I., and Kellis, M. (2011). PhyloCSF: a comparative genomics method to distinguish protein coding and non-coding regions. Bioinformatics *27*, i275-282. 10.1093/bioinformatics/btr209.
54. Stark, A., Lin, M.F., Kheradpour, P., Pedersen, J.S., Parts, L., Carlson, J.W., Crosby, M.A., Rasmussen, M.D., Roy, S., Deoras, A.N., et al. (2007). Discovery of functional elements in 12 Drosophila genomes using evolutionary signatures. Nature *450*, 219-232. 10.1038/nature06340.
55. Wang, D., Eraslan, B., Wieland, T., Hallstrom, B., Hopf, T., Zolg, D.P., Zecha, J., Asplund, A., Li, L.H., Meng, C., et al. (2019). A deep proteome and transcriptome abundance atlas of 29 healthy human tissues. Mol Syst Biol *15*, e8503. 10.15252/msb.20188503.
56. Giansanti, P., Samaras, P., Bian, Y., Meng, C., Coluccio, A., Frejno, M., Jakubowsky, H., Dobiasch, S., Hazarika, R.R., Rechenberger, J., et al. (2022). Mass spectrometry-based draft of the mouse proteome. Nat Methods *19*, 803-811. 10.1038/s41592-022-01526-y.
57. Phillips, P.C. (2008). Epistasis--the essential role of gene interactions in the structure and evolution of genetic systems. Nat Rev Genet *9*, 855-867. 10.1038/nrg2452.
58. Langfelder, P., and Horvath, S. (2008). WGCNA: an R package for weighted correlation network analysis. BMC Bioinformatics *9*, 559. 10.1186/1471-2105-9-559.
59. Zhang, J., and Xu, C. (2022). Gene product diversity: adaptive or not? Trends Genet *38*, 1112-1122. 10.1016/j.tig.2022.05.002.
60. Mao, Y., and Qian, S.B. (2024). Making sense of mRNA translational "noise". Semin Cell Dev Biol *154*, 114-122. 10.1016/j.semcdb.2023.03.004.
61. Broeils, L.A., Ruiz-Orera, J., Snel, B., Hubner, N., and van Heesch, S. (2023). Evolution and implications of de novo genes in humans. Nat Ecol Evol. 10.1038/s41559-023-02014-y.
62. Liu, X., Xiao, C., Xu, X., Zhang, J., Mo, F., Chen, J.Y., Delihas, N., Zhang, L., An, N.A., and Li, C.Y. (2024). Origin of functional de novo genes in humans from "hopeful monsters". Wiley Interdiscip Rev RNA *15*, e1845. 10.1002/wrna.1845.
63. Treichel, A.J., and Bazzini, A.A. (2022). Casting CRISPR-Cas13d to fish for microprotein functions in animal development. iScience *25*, 105547. 10.1016/j.isci.2022.105547.
64. Martin, M. (2011). Cutadapt removes adapter sequences from high-throughput sequencing reads. EMBnet. journal *17*, 10-12.
65. Cunningham, F., Allen, J.E., Allen, J., Alvarez-Jarreta, J., Amode, M.R., Armean, I.M., Austine-Orimoloye, O., Azov, A.G., Barnes, I., Bennett, R., et al. (2022). Ensembl 2022. Nucleic Acids Res *50*, D988-d995. 10.1093/nar/gkab1049.
66. Dobin, A., Davis, C.A., Schlesinger, F., Drenkow, J., Zaleski, C., Jha, S., Batut, P., Chaisson, M., and Gingeras, T.R. (2013). STAR: ultrafast universal RNA-seq aligner. Bioinformatics *29*, 15-21. 10.1093/bioinformatics/bts635.
67. Chang, Y., Lei, T., and Zhang, H. (2023). PSite: inference of read-specific P-site offsets for

ribosomal footprints. bioRxiv, 2023.2006.2027.546788. 10.1101/2023.06.27.546788.
68. Tierney, J.A.S., Świrski, M.I., Tjeldnes, H., Kiran, A.M., Carancini, G., Kiniry, S.J., Michel, A.M., Kufel, J., Valen, E., and Baranov, P.V. (2025). RiboSeq.Org: an integrated suite of resources for ribosome profiling data analysis and visualization. Nucleic Acids Res *53*, D268-d274. 10.1093/nar/gkae1020.
69. Nassar, L.R., Barber, G.P., Benet-Pagès, A., Casper, J., Clawson, H., Diekhans, M., Fischer, C., Gonzalez, J.N., Hinrichs, A.S., Lee, B.T., et al. (2023). The UCSC Genome Browser database: 2023 update. Nucleic Acids Res *51*, D1188-d1195. 10.1093/nar/gkac1072.
70. Rodriguez, J.M., Pozo, F., Cerdán-Vélez, D., Di Domenico, T., Vázquez, J., and Tress, M.L. (2022). APPRIS: selecting functionally important isoforms. Nucleic Acids Res *50*, D54-d59. 10.1093/nar/gkab1058.
71. Lorenz, R., Bernhart, S.H., Höner Zu Siederdissen, C., Tafer, H., Flamm, C., Stadler, P.F., and Hofacker, I.L. (2011). ViennaRNA Package 2.0. Algorithms Mol Biol *6*, 26. 10.1186/1748-7188-6-26.
72. Liu, M., Zi, B., Zhang, H., and Zhang, H. (2024). cubar: a versatile package for codon usage bias analysis in R. R package *version 1.1*. 10.5281/zenodo.10155990.
73. Chan, P.P., and Lowe, T.M. (2016). GtRNAdb 2.0: an expanded database of transfer RNA genes identified in complete and draft genomes. Nucleic Acids Res *44*, D184-189. 10.1093/nar/gkv1309.
74. Jones, P., Binns, D., Chang, H.Y., Fraser, M., Li, W., McAnulla, C., McWilliam, H., Maslen, J., Mitchell, A., Nuka, G., et al. (2014). InterProScan 5: genome-scale protein function classification. Bioinformatics *30*, 1236-1240. 10.1093/bioinformatics/btu031.
75. Quinlan, A.R., and Hall, I.M. (2010). BEDTools: a flexible suite of utilities for comparing genomic features. Bioinformatics *26*, 841-842. 10.1093/bioinformatics/btq033.
76. Erdős, G., Pajkos, M., and Dosztányi, Z. (2021). IUPred3: prediction of protein disorder enhanced with unambiguous experimental annotation and visualization of evolutionary conservation. Nucleic Acids Res *49*, W297-w303. 10.1093/nar/gkab408.
77. Dalla, V., Giraitis, L., and Phillips, P.C.B. (2022). obust Tests for White Noise and Cross-Correlation. Econometric Theory *38*, 913-941. 10.1017/S0266466620000341.
78. Katoh, K., and Standley, D.M. (2013). MAFFT multiple sequence alignment software version 7: improvements in performance and usability. Mol Biol Evol *30*, 772-780. 10.1093/molbev/mst010.
79. Lemoine, F., and Gascuel, O. (2021). Gotree/Goalign: toolkit and Go API to facilitate the development of phylogenetic workflows. NAR Genom Bioinform *3*, lqab075. 10.1093/nargab/lqab075.
80. Ashkenazy, H., Penn, O., Doron-Faigenboim, A., Cohen, O., Cannarozzi, G., Zomer, O., and Pupko, T. (2012). FastML: a web server for probabilistic reconstruction of ancestral sequences. Nucleic Acids Res *40*, W580-584. 10.1093/nar/gks498.
81. Paradis, E., and Schliep, K. (2019). ape 5.0: an environment for modern phylogenetics and evolutionary analyses in R. Bioinformatics *35*, 526-528. 10.1093/bioinformatics/bty633.
82. Pockrandt, C., Steinegger, M., and Salzberg, S.L. (2022). PhyloCSF++: a fast and user-friendly implementation of PhyloCSF with annotation tools. Bioinformatics *38*, 1440-1442. 10.1093/bioinformatics/btab756.
83. Love, M.I., Huber, W., and Anders, S. (2014). Moderated estimation of fold change and dispersion for RNA-seq data with DESeq2. Genome Biol *15*, 550. 10.1186/s13059-014-0550-8.
84. Kryuchkova-Mostacci, N., and Robinson-Rechavi, M. (2017). A benchmark of gene expression tissue-specificity metrics. Brief Bioinform *18*, 205-214. 10.1093/bib/bbw008.
85. Patro, R., Duggal, G., Love, M.I., Irizarry, R.A., and Kingsford, C. (2017). Salmon provides fast and bias-aware quantification of transcript expression. Nat Methods *14*, 417-419. 10.1038/nmeth.4197.
86. Rezaie, N., Reese, F., and Mortazavi, A. (2023). PyWGCNA: a Python package for weighted gene co-expression network analysis. Bioinformatics *39*. 10.1093/bioinformatics/btad415.
87. Traag, V.A., Waltman, L., and van Eck, N.J. (2019). From Louvain to Leiden: guaranteeing well-connected communities. Sci Rep *9*, 5233. 10.1038/s41598-019-41695-z.

88. Csárdi, G., Nepusz, T., Traag, V., Horvát, S., Zanini, F., Noom, D., and Müller, K. (2024). igraph: Network Analysis and Visualization in R. R package *version 2.1.3*. 10.5281/zenodo.7682609.
89. Wu, T., Hu, E., Xu, S., Chen, M., Guo, P., Dai, Z., Feng, T., Zhou, L., Tang, W., Zhan, L., et al. (2021). clusterProfiler 4.0: A universal enrichment tool for interpreting omics data. Innovation (Camb) *2*, 100141. 10.1016/j.xinn.2021.100141.

775 **Figures**

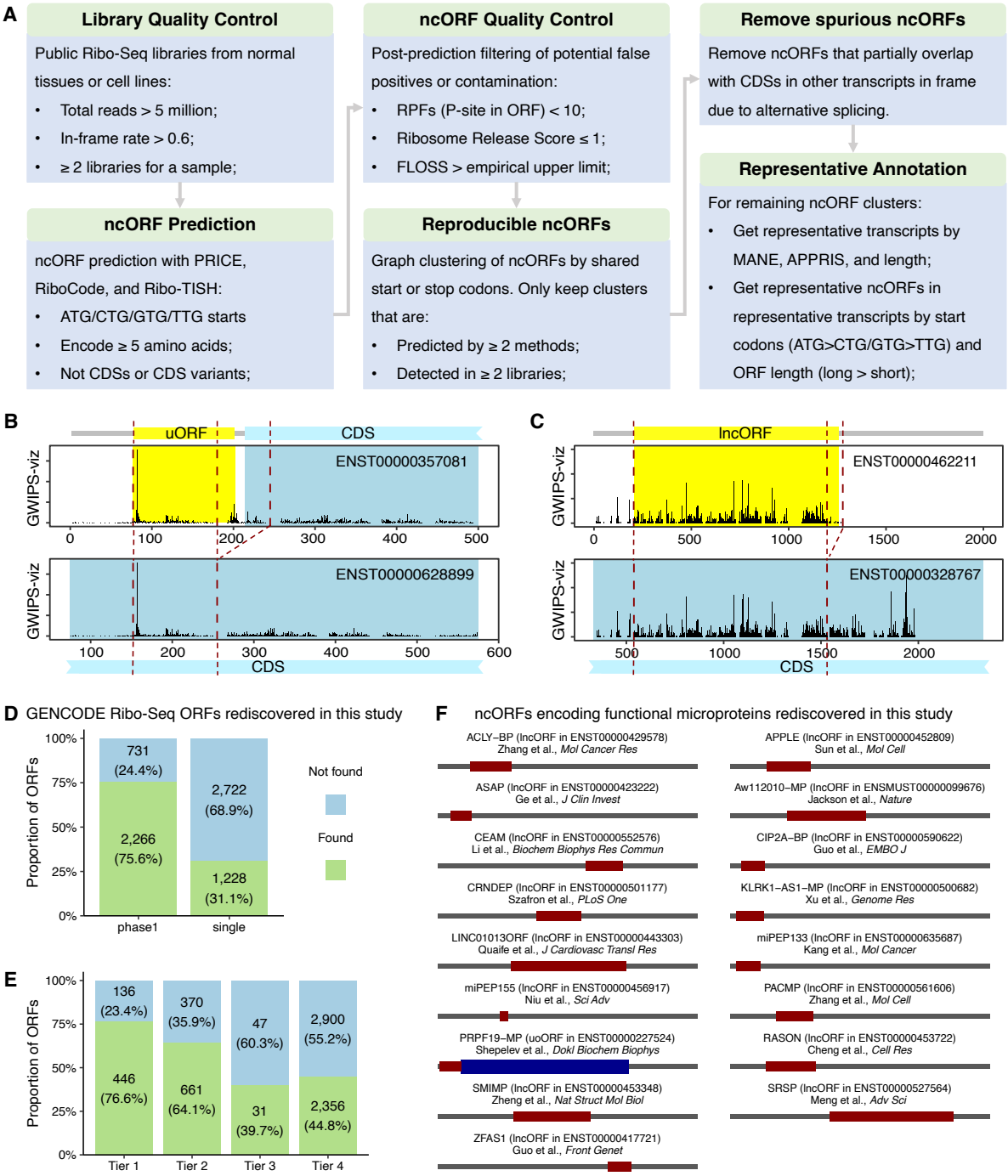

776

777 **Figure 1. Annotation of ncORFs in humans and mice.**

778 (**A**) Overview of the integrative pipeline for ncORF annotation in human and mouse genomes. (**B-C**)
779 RPF coverage plot for a representative uORF (B) and a lncORF (C), visualized using the Ribo-Seq
780 signal track from GWIPS-viz[68]. ncORFs were shown in yellow and CDSs in cyan. Dashed lines indicate
781 identical genomic regions shared across transcript isoforms. (**D-E**) Proportion of GENCODE ncORFs
782 rediscovered in this study. GENCODE ncORFs were stratified either by reproducibility across
783 independent studies (D) or by tiered translation evidence strength (E). (**F**) Known ncORFs that were
784 experimentally characterized in earlier studies and independently rediscovered in this study from

humans and mice. CDS, coding sequence; FLOSS, fragment length organization similarity score; MANE, matched annotation from NCBI and EBI; ncORF, non-canonical open reading frame; ORF, open reading frame; RPF, ribosome-protected fragment.

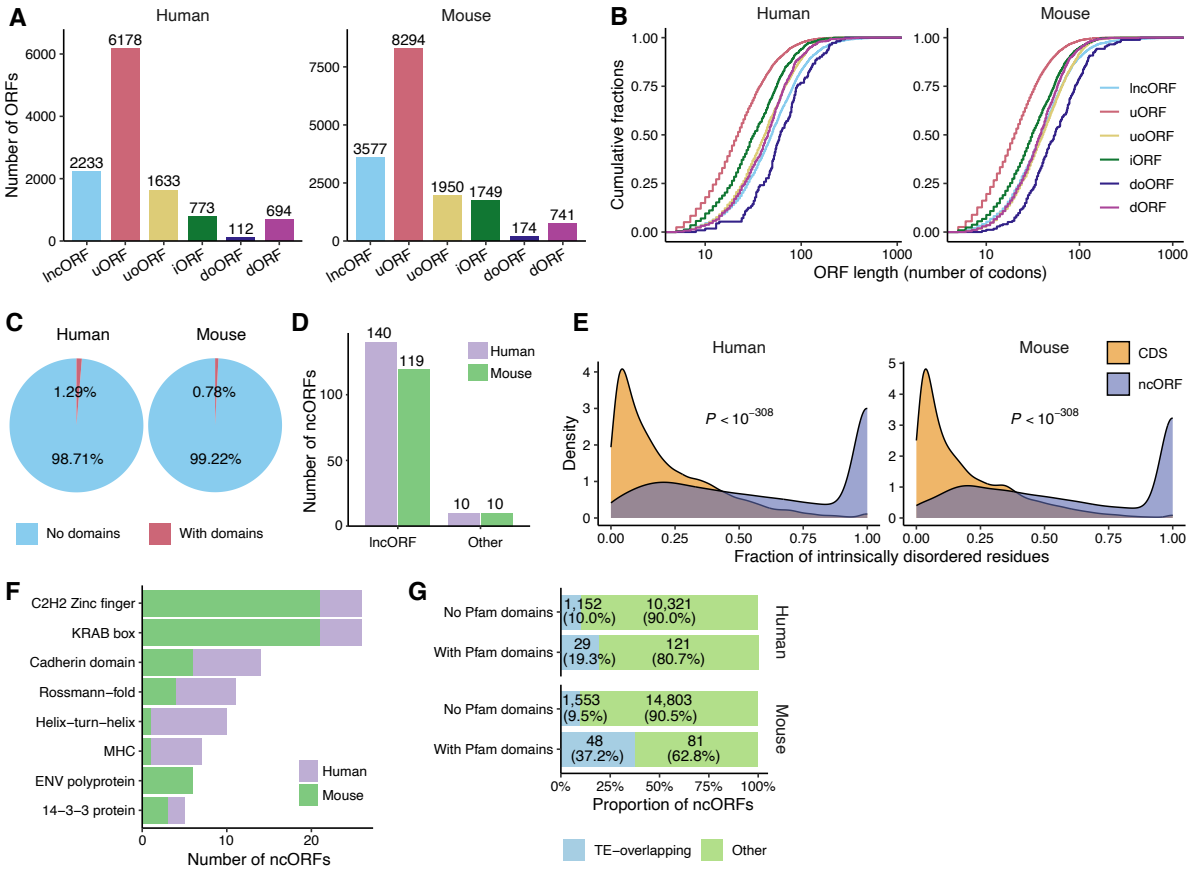

Figure 2. Sequence features of ncORFs and putative ncEPs in humans and mice.
(**A**) Number of ncORFs belonging to different categories. (**B**) Distribution of ncORF lengths. (**C**) Proportion of ncEPs that contain known Pfam domains. (**D**) Number of ncORFs with Pfam domains among lncORFs and other ncORF categories. (**E**) Distribution of the proportion of intrinsically disordered residues in CDS- and ncORF-encoded proteins. (**F**) Most frequently identified Pfam domains among human and mouse ncORFs. (**G**) Proportion of ncORFs overlapping with TEs, stratified by presence or absence of Pfam domains. Differences were assessed using Wilcoxon rank-sum tests. CDS, coding sequence; ncORF, non-canonical open reading frame; ncEP, ncORF-encoded protein; TE, transposable element.

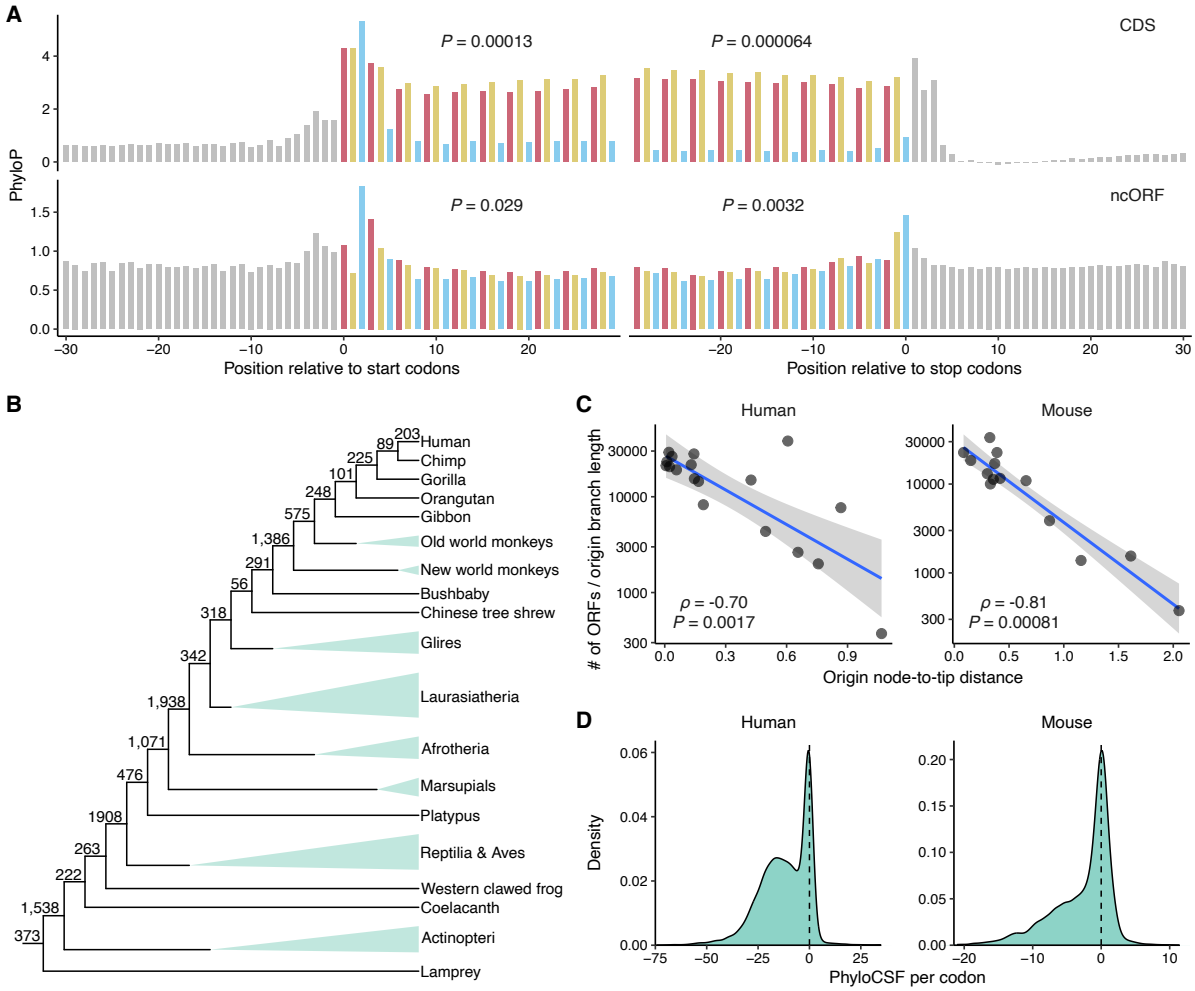

Figure 3. Evolutionary constraints of ncORFs.

(**A**) The mean PhyloP scores of 30 base pairs upstream and downstream of the ORF start or stop codons in mammals. Codons were delineated with bars of alternating colors by different frames, and nucleotides in untranslated regions were shown in grey. The significance of three-nucleotide periodicity was assessed by autocorrelation with a lag of three. (**B**) Cladograms of vertebrates with the number of ncORFs originating at each ancestral branch of humans. Triangles indicate species merged into larger clade for visual simplicity. (**C**) Relationship between ORF origination rates and node ages measured as node-to-tip distances. Origination rate was defined as the number of ncORFs that originated on a branch divided by the branch length. Blue lines show linear regression fits, and grey bands represent 95% prediction confidence intervals. Spearman's correlation is indicated. (**D**) Distribution of ncORF PhyloCSF scores normalized by the number of codons in per ncORF. The dashed line denotes zero. CDS, coding sequence; ncORF, non-canonical open reading frame; ORF, open reading frame.

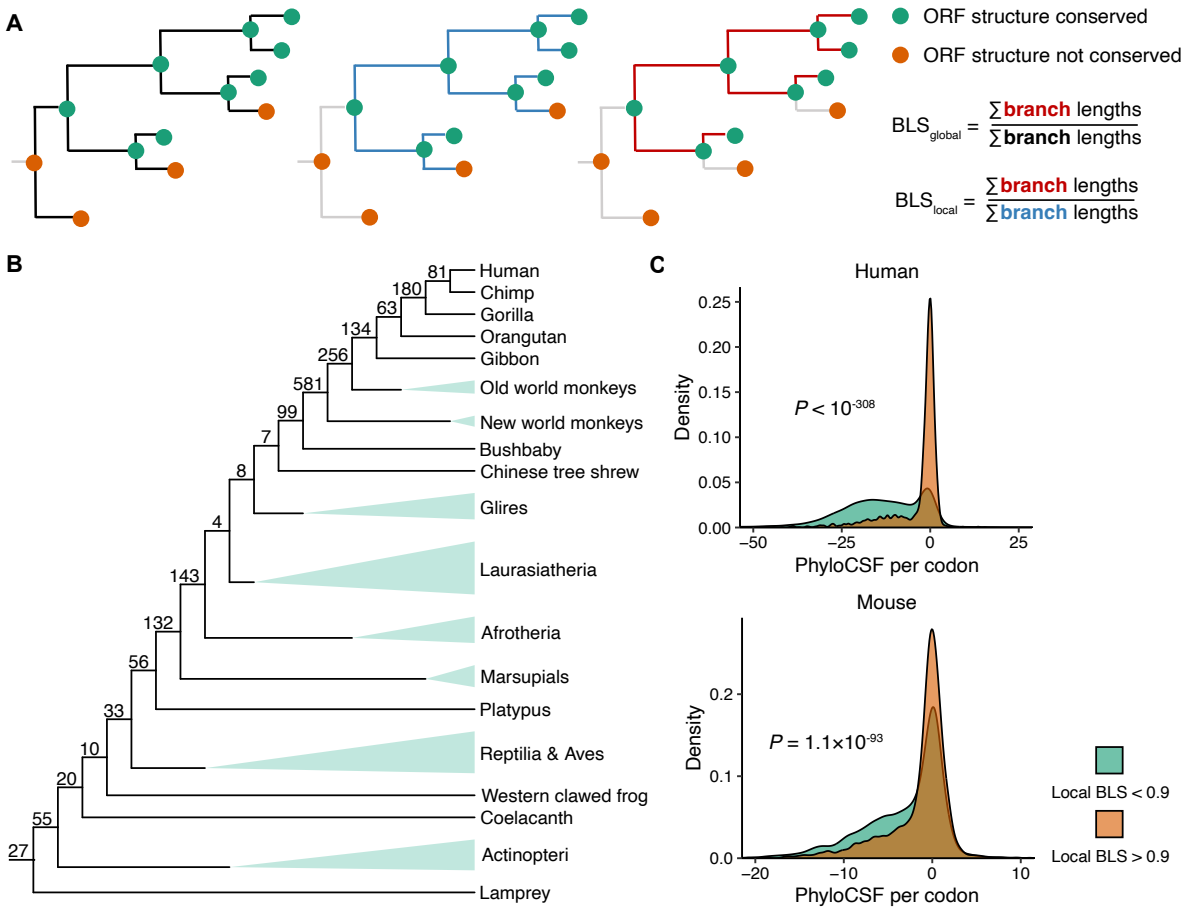

Figure 4. Lineage-specifically conserved ncORFs.

(**A**) Schematic illustration for BLS calculation. (**B**) Cladograms of vertebrates showing the number of lineage-specifically conserved ncORFs (local BLS > 0.9) at each ancestral node for humans and mice. (**C**) Distribution of PhyloCSF scores per codon for lineage-specifically conserved ncORFs compared to all other ncORFs. BLS, branch length score; ncORF, non-canonical open reading frame; ORF, open reading frame.

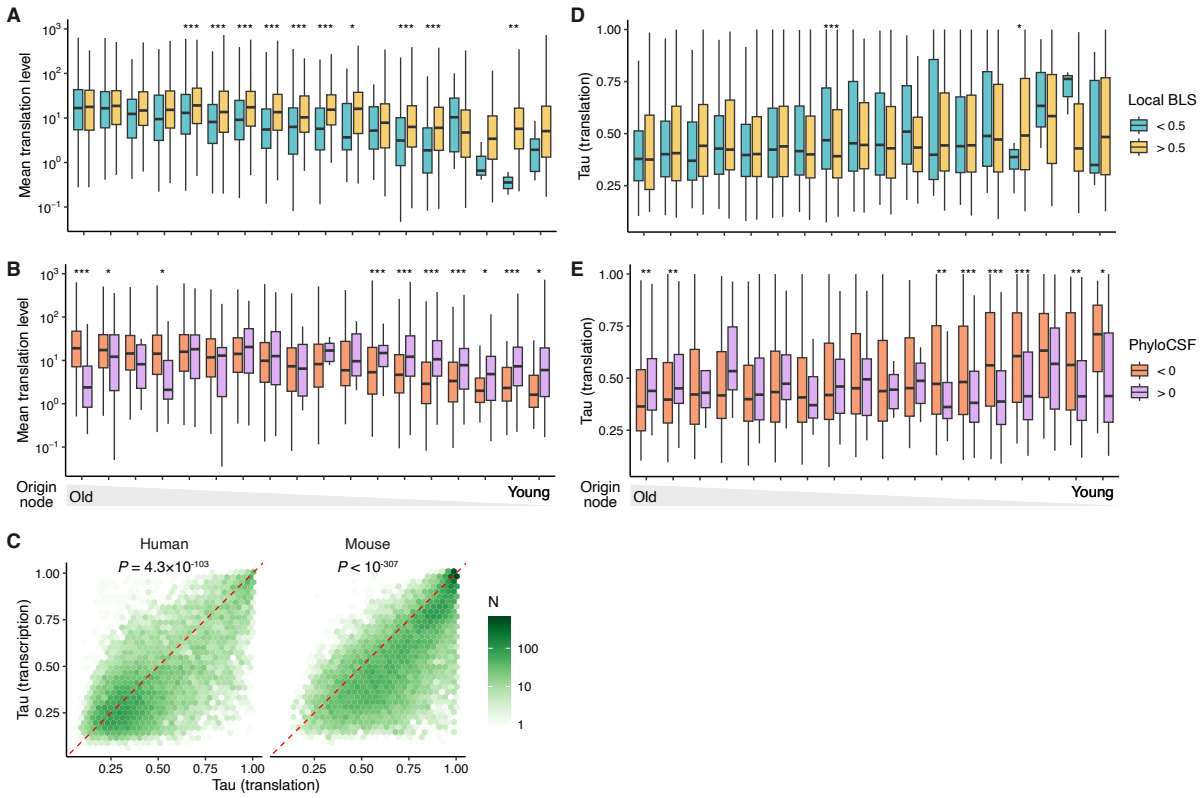

Figure 5. Evolutionary dynamics of ncORF expression.

(**A**) Distribution of mean translation levels of human ncORFs grouped by their origin nodes and further stratified by local BLS. Statistical significance was assessed using Wilcoxon rank-sum tests. ***, $P < 0.001$; **, $P < 0.01$; *, $P < 0.05$. (**B**) Similar to (A) but ncORFs are further stratified by local BLS. (**C**) Relationship between ncORF tissue specificity at translation and transcription levels. Differences were determined with Wilcoxon signed-rank tests. (**D-E**) Similar to (A) and (B) but showing the distribution of tissue specificity at the translation level. CDS, coding sequence; ncORF, non-canonical open reading frame; ORF, open reading frame.

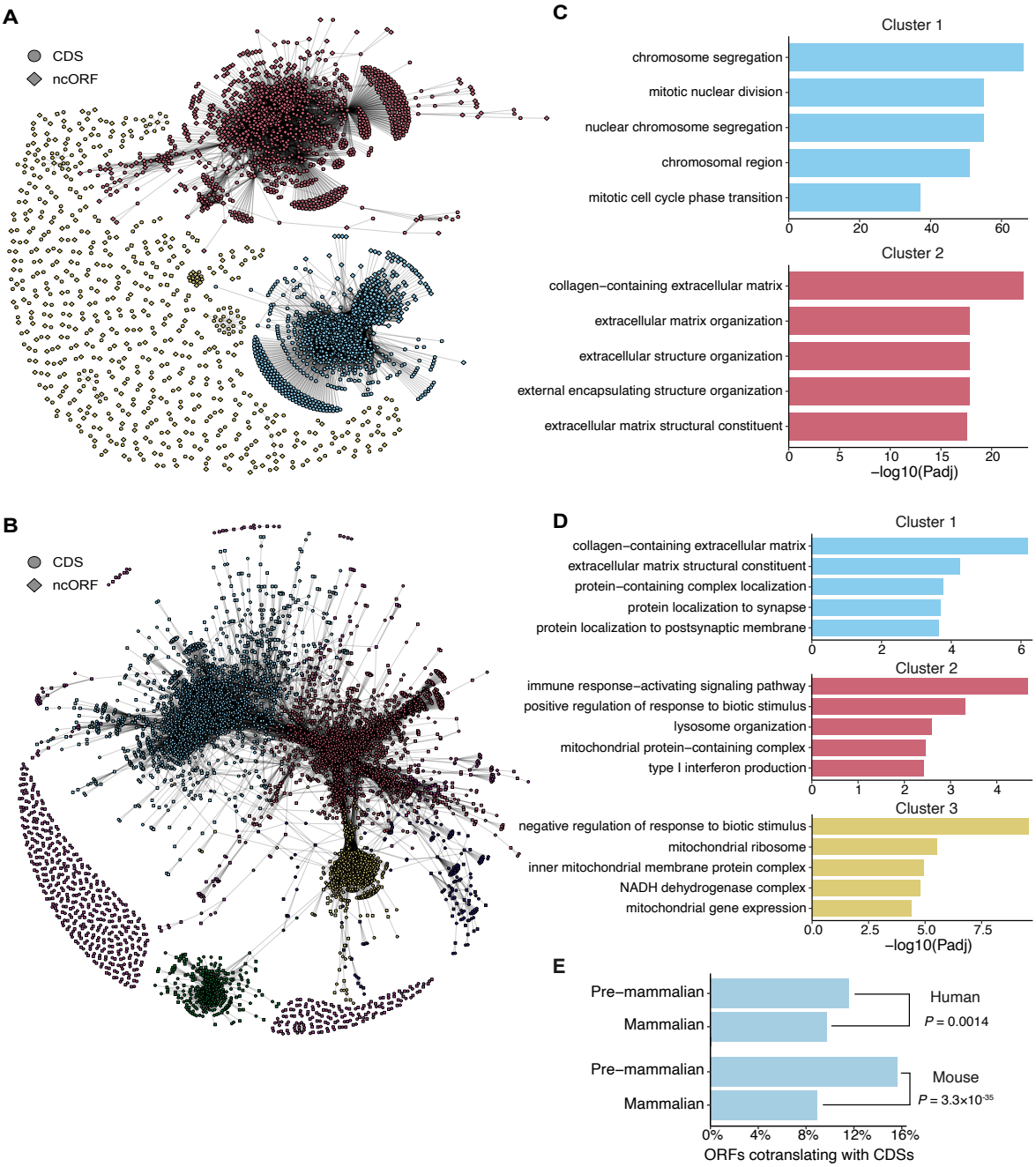

Figure 6. ncORF-CDS co-translation network.

(**A**) Bipartite network of ncORF-CDS co-translation in humans. (**B**) Bipartite network of ncORF-CDS co-translation in mice. ncORFs and CDSs are represented by different shapes and colored according to their cluster membership. Only the largest clusters were highlighted (top two in humans and top five in mice). (**C**) Top five enriched gene ontology terms for each of the two largest clusters in the human network shown in (A). (**D**) Top five enriched gene ontology terms for each of the three largest clusters in the mouse network shown in (B). (**E**) Proportion of ncORFs cotranslating with CDSs among ancient (pre-mammalian origin) versus younger (mammalian-specific) ncORFs. Differences were tested with Fisher's exact tests. CDS, coding sequence; ncORF, non-canonical open reading frame; ORF, open reading frame.

Supplementary Information

Supplementary Figures

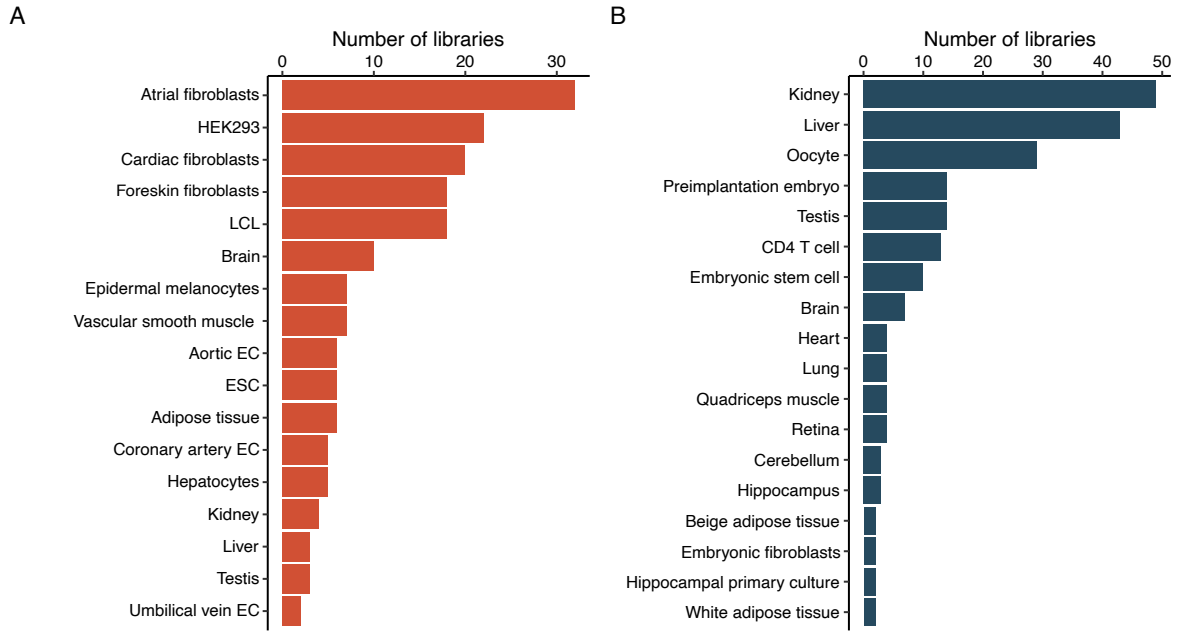

Supplementary figure 1. Number of high-quality Ribo-Seq libraries passing quality control for each sample in humans (A) and mice (B). EC, endothelial cell; ESC, embryonic stem cell; LCL, lymphoblastoid cell line; Ribo-Seq, ribosome profiling.

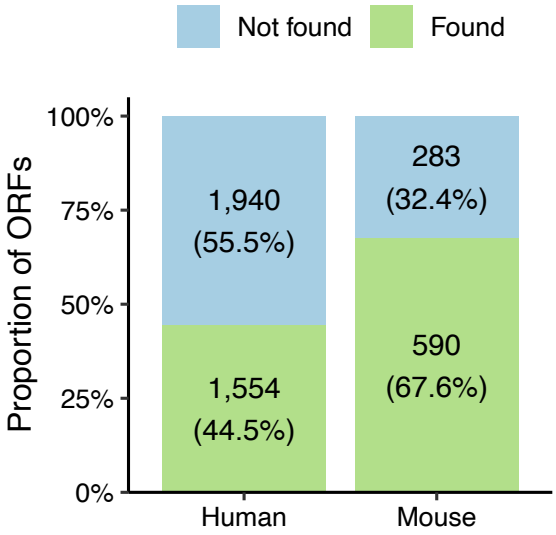

Supplementary figure 2. Rediscovery rate of non-canonical ORFs supported by MS evidence, as compiled in our previous study[1]. MS, mass spectrometry; ORF, open reading frame.

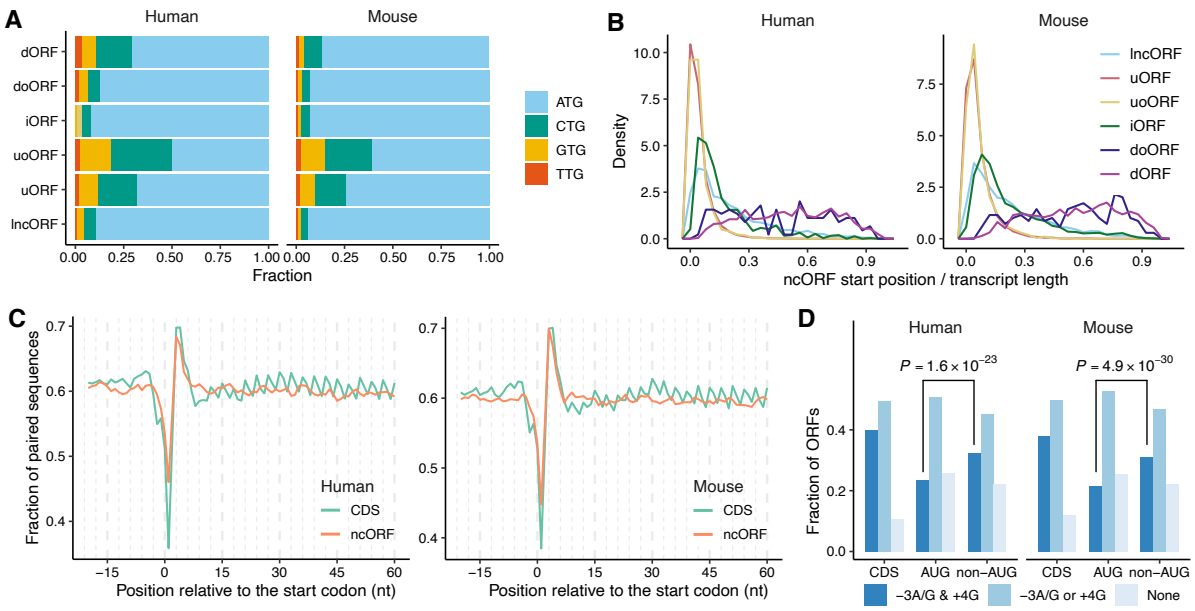

Supplementary figure 3. Translation-related signatures of ncORF sequences. (**A**) Start codon usage among ncORFs. (**B**) Distribution of relative start positions of ncORFs within transcripts. The *x*-axis represents the position of ncORF start codon normalized by transcript length. (**C**) Nucleotide pairing probabilities around the start codons of ncORFs and CDSs. (**D**) Proportion of ncORFs with different Kozak sequence contexts. Statistical significance was assessed using Fisher's exact test. CDS, coding sequence; ncORF, non-canonical open reading frame; ORF, open reading frame.

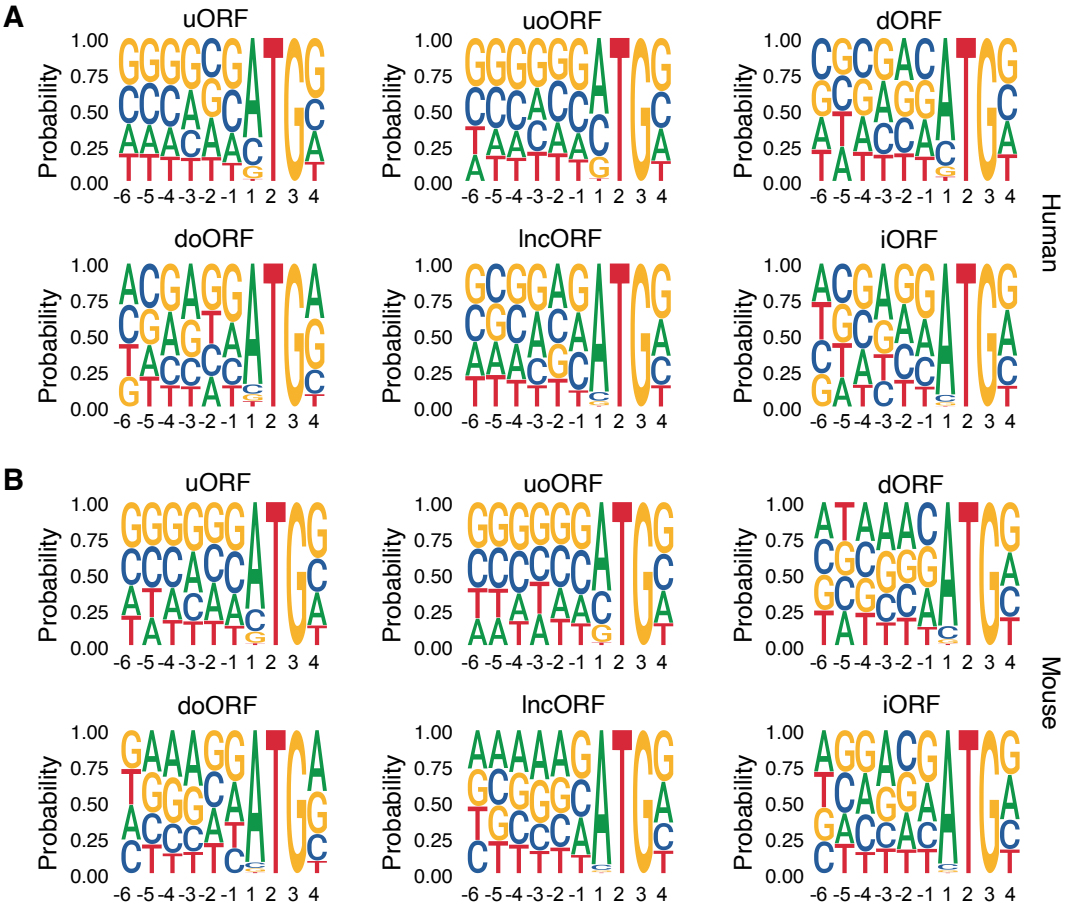

Supplementary figure 4. Seqlogo plots of Kozak sequence context surrounding ncORF start codons in humans (A) and mice (B). The first nucleotide of the start codon is designated as position +1. The height of each nucleotide at each position reflects its frequency. ncORF, non-canonical open reading frame.

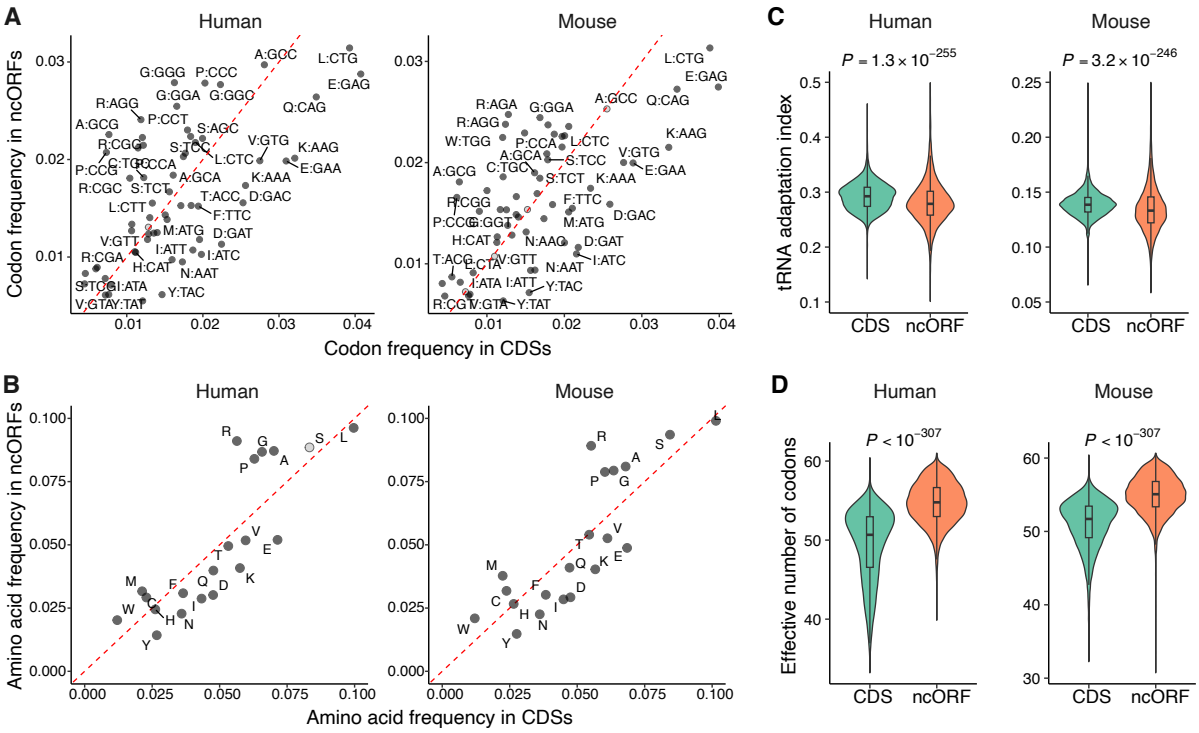

Supplementary figure 5. Differences in codon and amino acid usage between ncORFs and CDSs. **(A-B)** Differences in relative usage of codons (A) and amino acids (B). Significance was determined using Fisher's exact tests and corrected for multiple-testing. Codons or amino acids with adjusted *P* value < 0.05 are shown in dark grey. (**C-D**) Distribution of tRNA adaptation index values (C) and effective number of codons (D) for CDSs and ncORFs. Statistical significance was determined by Wilcoxon rank-sum tests. CDS, coding sequence; ncORF, non-canonical open reading frame.

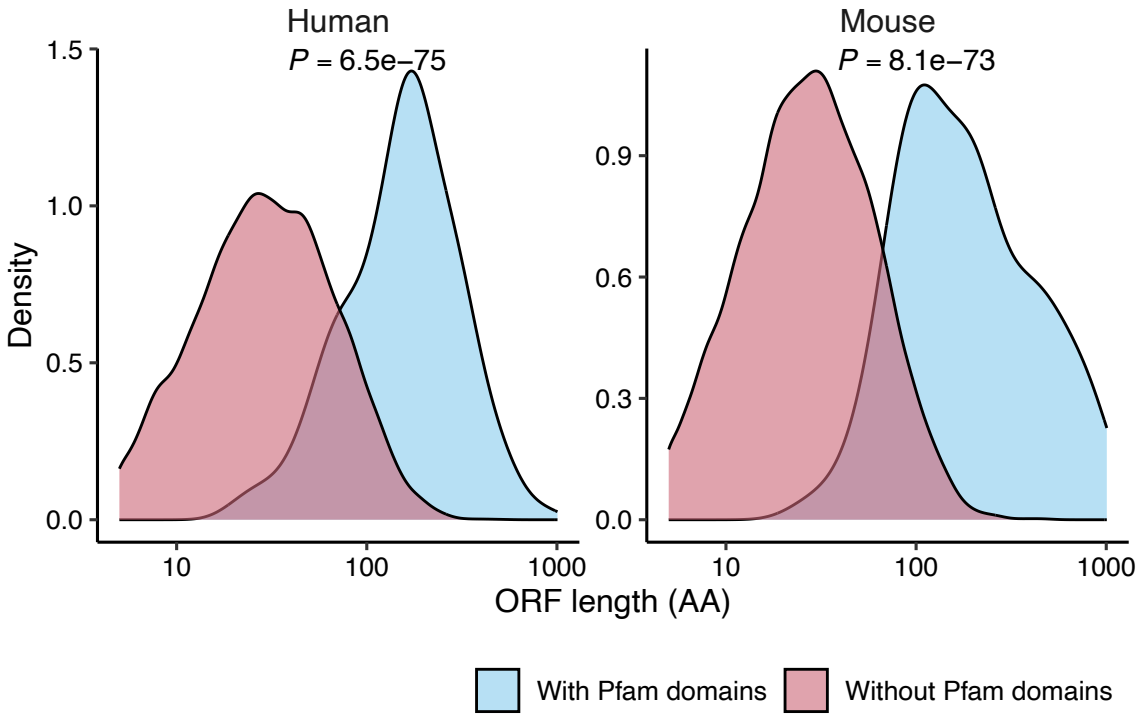

Supplementary figure 6. Length distribution of ncORFs with (blue) or without (red) known Pfam domains. Statistical differences were assessed using Wilcoxon rank-sum tests. AA, amino acid; ncORF, non-canonical open reading frame; ORF, open reading frame.

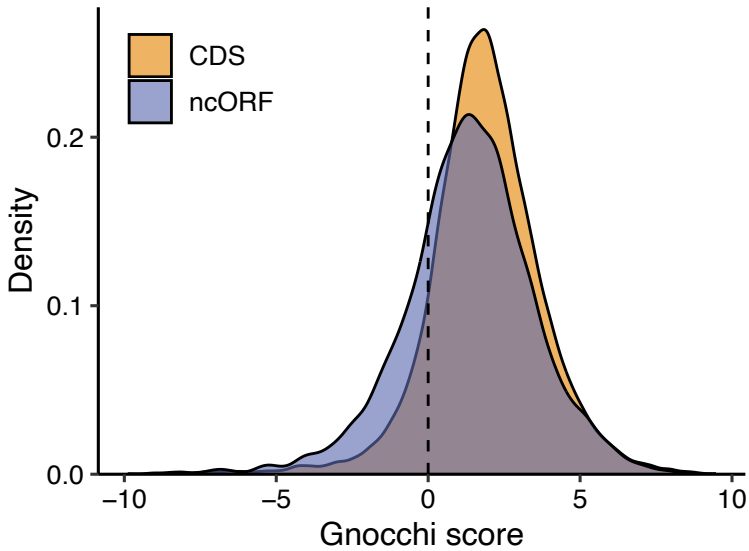

Supplementary figure 7. Distribution of Gnocchi scores for CDSs and ncORFs. Statistical significance of deviation from zero was assessed using Wilcoxon signed-rank tests. CDS, coding sequence; Gnocchi, Genomic Non-Coding Constraint of Haplo-Insufficient variation; ncORF, non-canonical open reading frame.

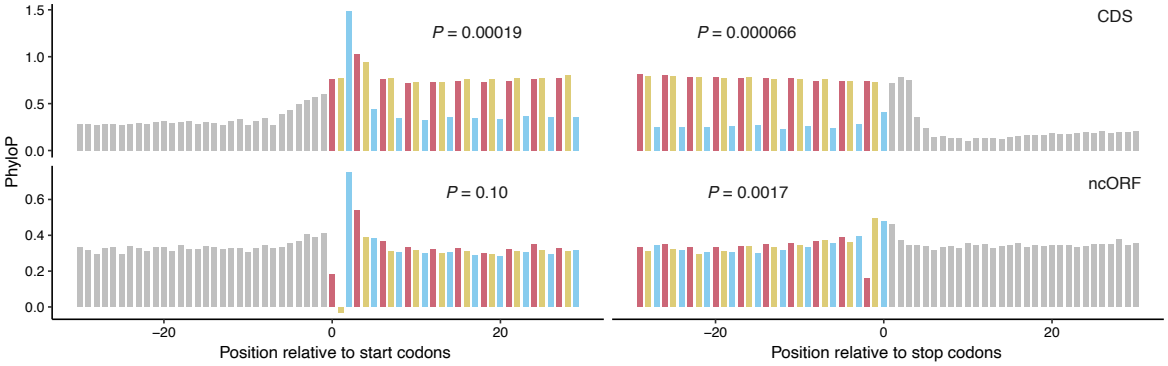

Supplementary figure 8. The mean PhyloP score of 30 base pairs upstream and downstream of the ORF (CDS or ncORF) start or stop codons in primates. Codons were delineated with bars of alternating colors for different frames, and nucleotides in untranslated regions were shown in grey. Statistical significance of the three-nucleotide periodicity was determined by autocorrelation with a lag of three. CDS, coding sequence; ncORF, non-canonical open reading frame.

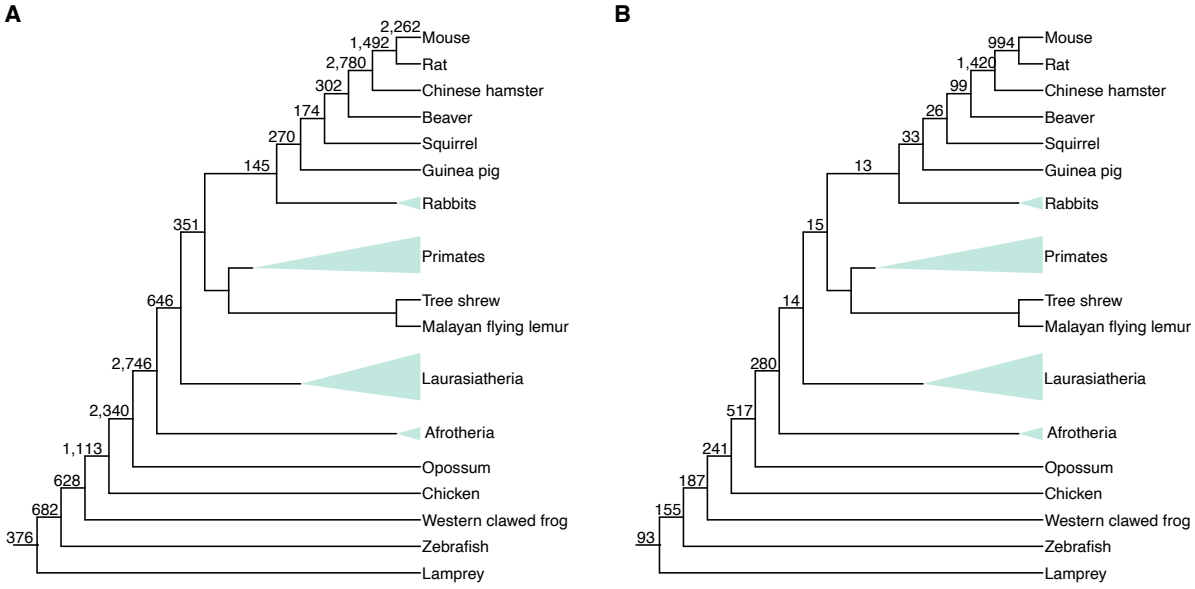

Supplementary figure 9. Cladograms of vertebrates showing the number of ncORFs originating at each ancestral branch leading to mice. (**A**) All ncORFs. (**B**) Lineage-specific ncORFs with local branch length score > 0.9. Triangles indicate species merged into larger clades for visual simplicity.

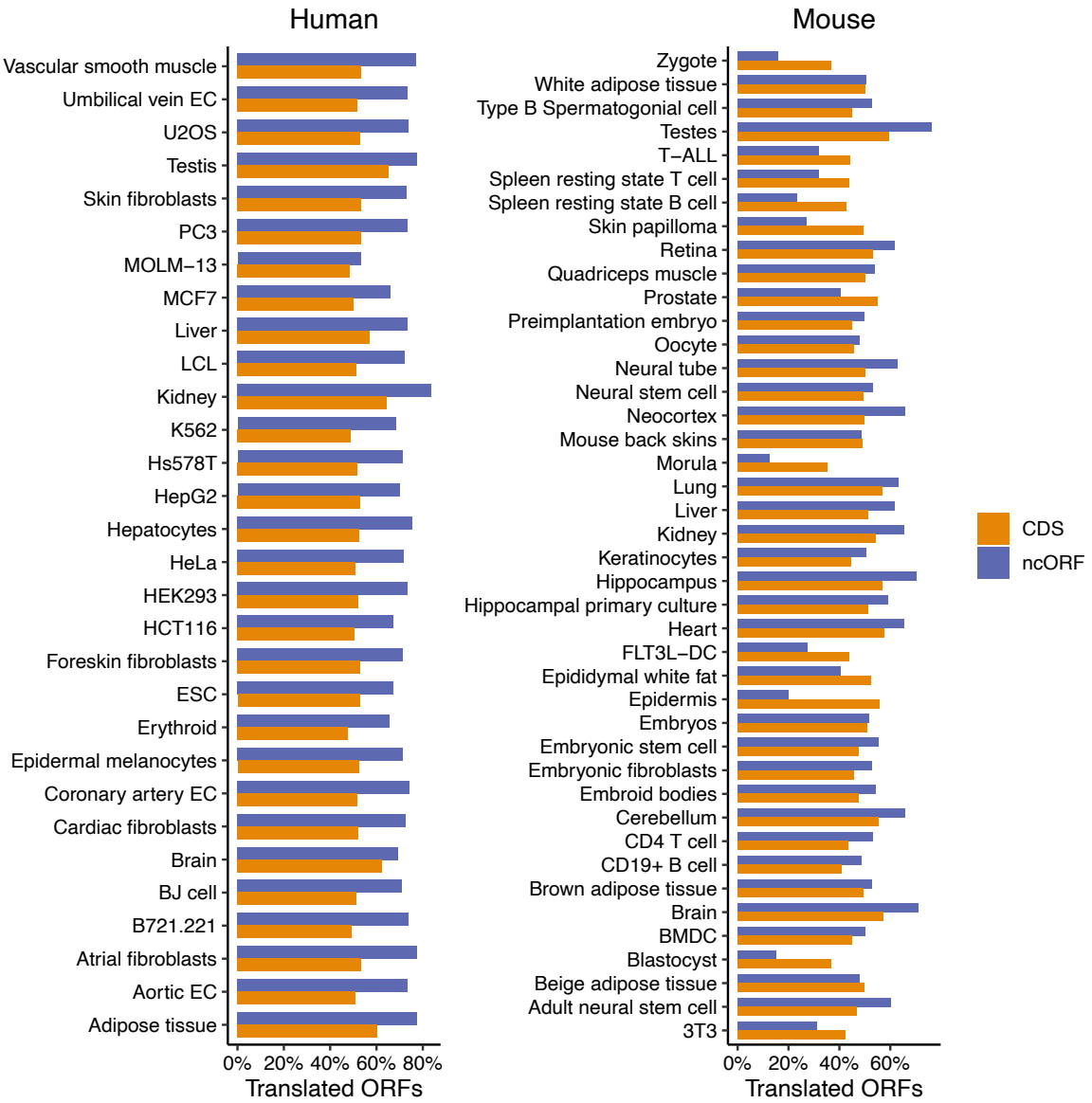

Supplementary figure 10. Proportion of translated ncORFs and CDSs detected in each human and mouse sample. Translated ORFs were detected with RPKM ≥ 1. BMDC, bone marrow-derived dendritic cell; CDS, coding sequence; DC, dendritic cell; EC, endothelial cell; ESC, embryonic stem cell; LCL, lymphoblastoid cell line; ncORF, non-canonical open reading frame; RPKM, reads per kilobase per million mapped reads; T-ALL, T-cell acute lymphoblastic leukemia.

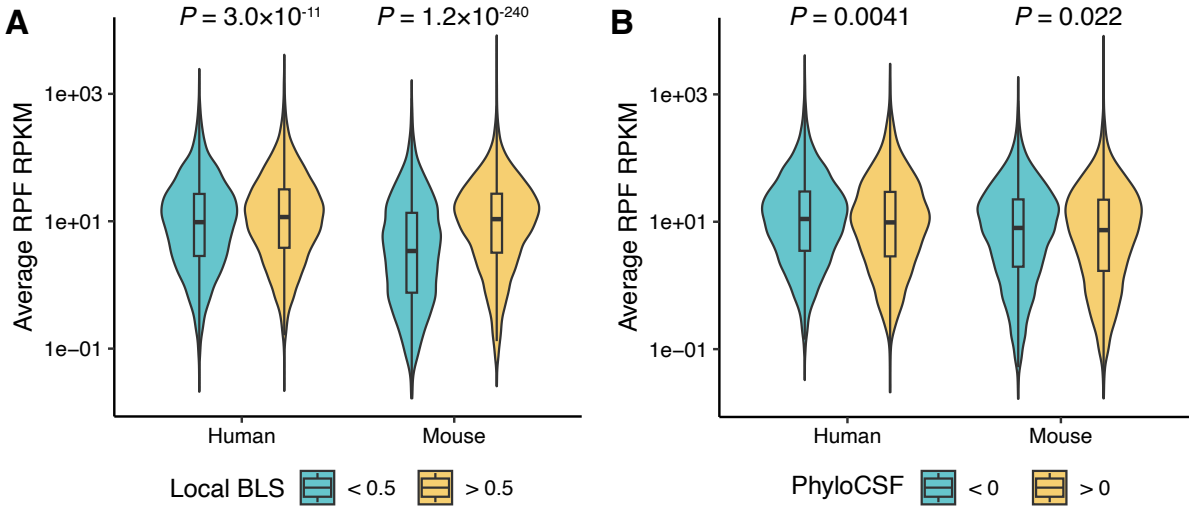

Supplementary figure 11. Distribution of average translation levels of ncORFs stratified by local BLS (A) or PhyloCSF (B) in humans and mice. Statistical differences were assessed using Wilcoxon rank-sum tests. BLS, branch length score; ncORF, non-canonical open reading frame; RPF, ribosome-protected fragment; RPKM, reads per kilobase per million mapped reads.

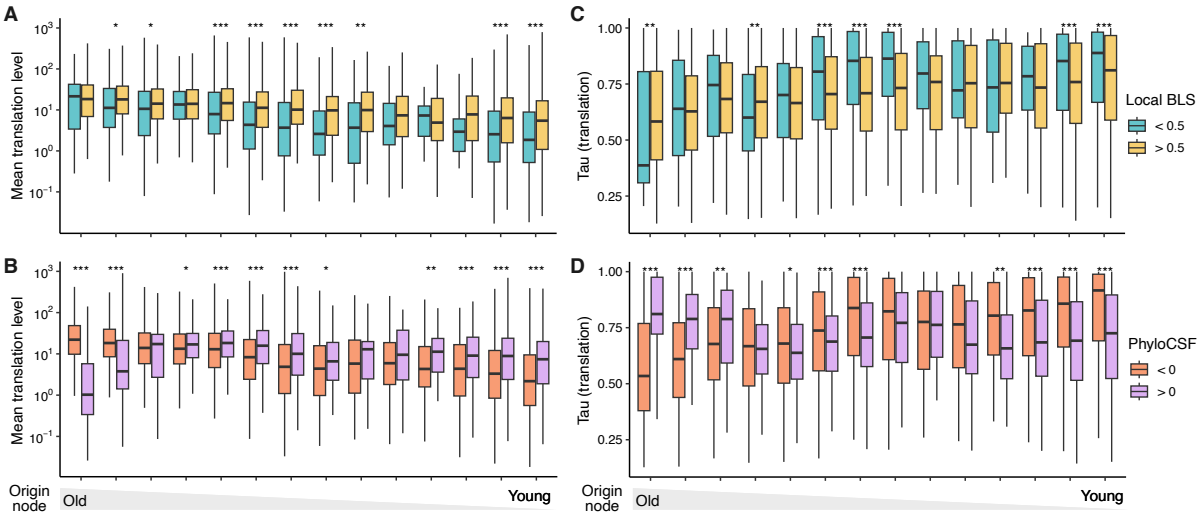

Supplementary figure 12. Expression patterns of ncORFs in mice. (**A**) Distribution of mean translation levels of mouse ncORFs grouped by origin nodes and further stratified by local BLS. Statistical significance was assessed with Wilcoxon rank-sum tests. ***, $P < 0.001$; **, $P < 0.01$; *, $P < 0.05$. (**B**) Similar to (A) but ncORFs are further stratified by PhyloCSF scores. (**C-D**) Similar to (A) and (B), but showing the distribution of tissue-specificity at the translation level.

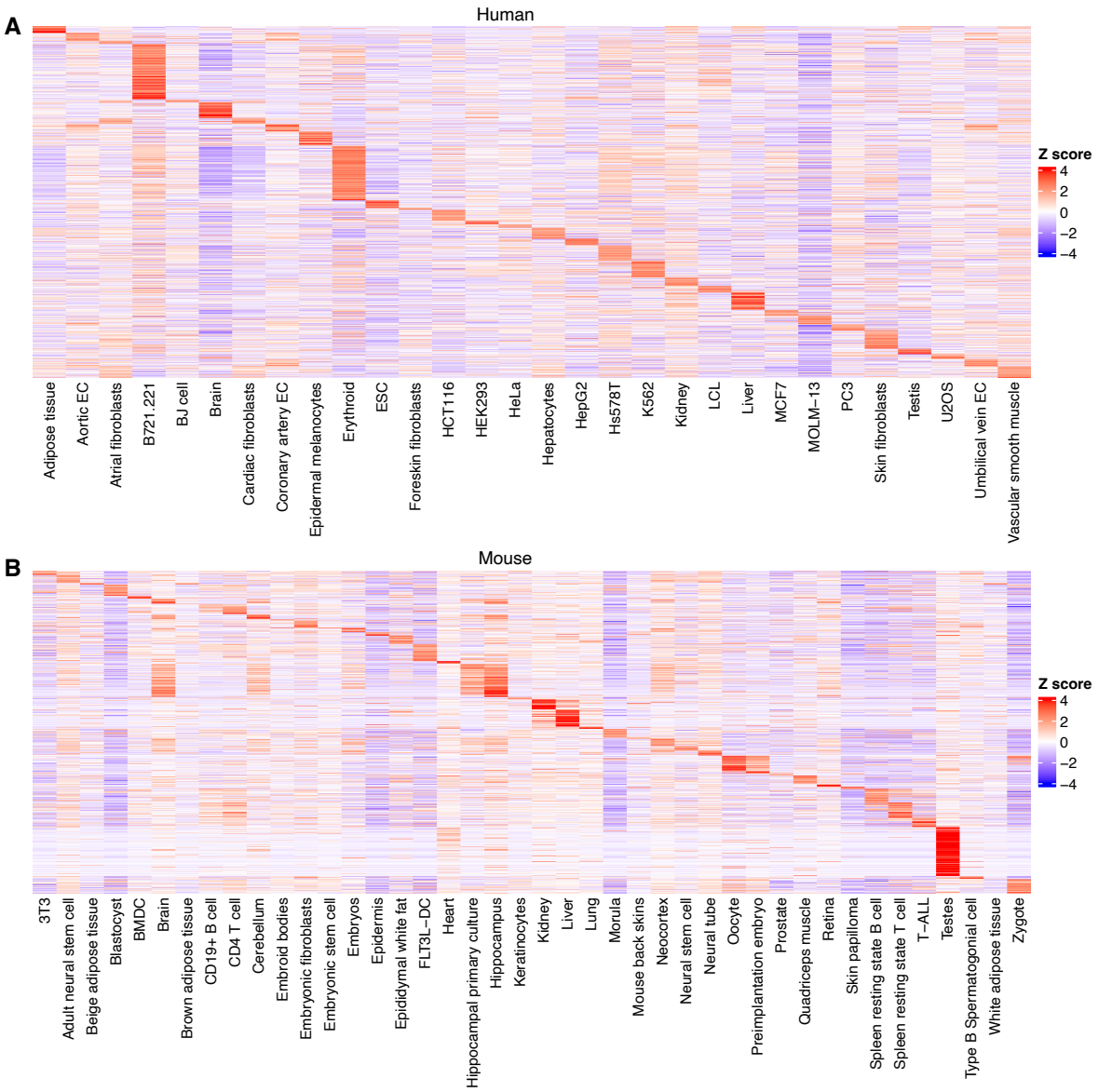

Supplementary figure 13. Heatmap showing the translation levels of ncORFs in human (A) and mouse (B) samples. Only ncORFs with translation level (RPKM) ≥ 1 in at least one sample are displayed. Translation levels were normalized across samples by Z-score transformation before visualization. BMDC, bone marrow-derived dendritic cell; DC, dendritic cell; EC, endothelial cell; ESC, embryonic stem cell; LCL, lymphoblastoid cell line; ncORF, non-canonical open reading frame; Ribo-Seq, ribosome profiling; RPKM, reads per kilobase per million mapped reads; T-ALL, T-cell acute lymphoblastic leukemia.

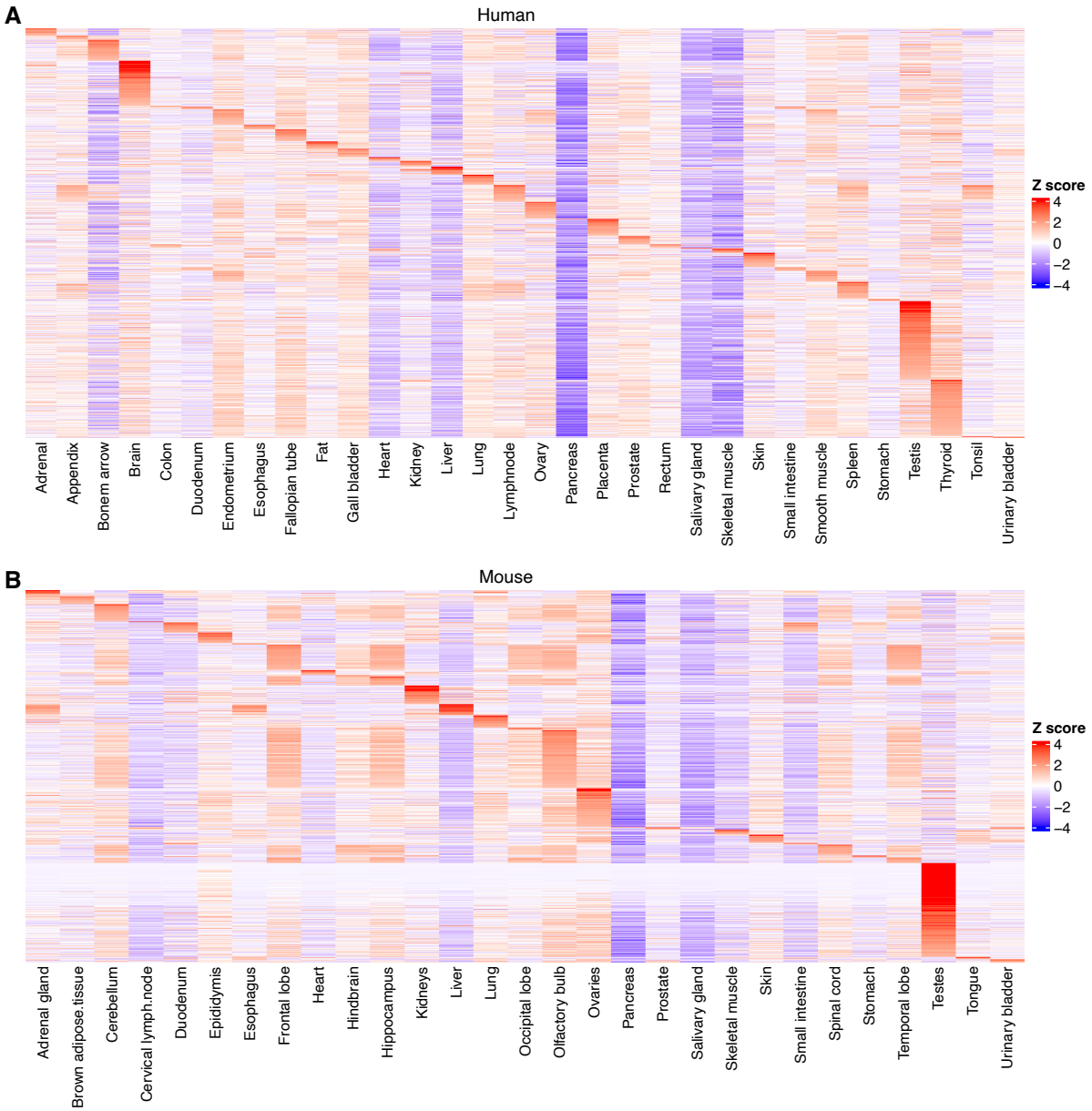

Supplementary figure 14. Heatmap showing the transcription levels of ncORF-containing genes in humans (A) and mice (B). Only genes expressed with TPM ≥ 1 in at least one sample are shown. TPM values were normalized across samples by Z-score transformation prior to visualization. ncORF, non-canonical open reading frame; TPM, transcripts per million.

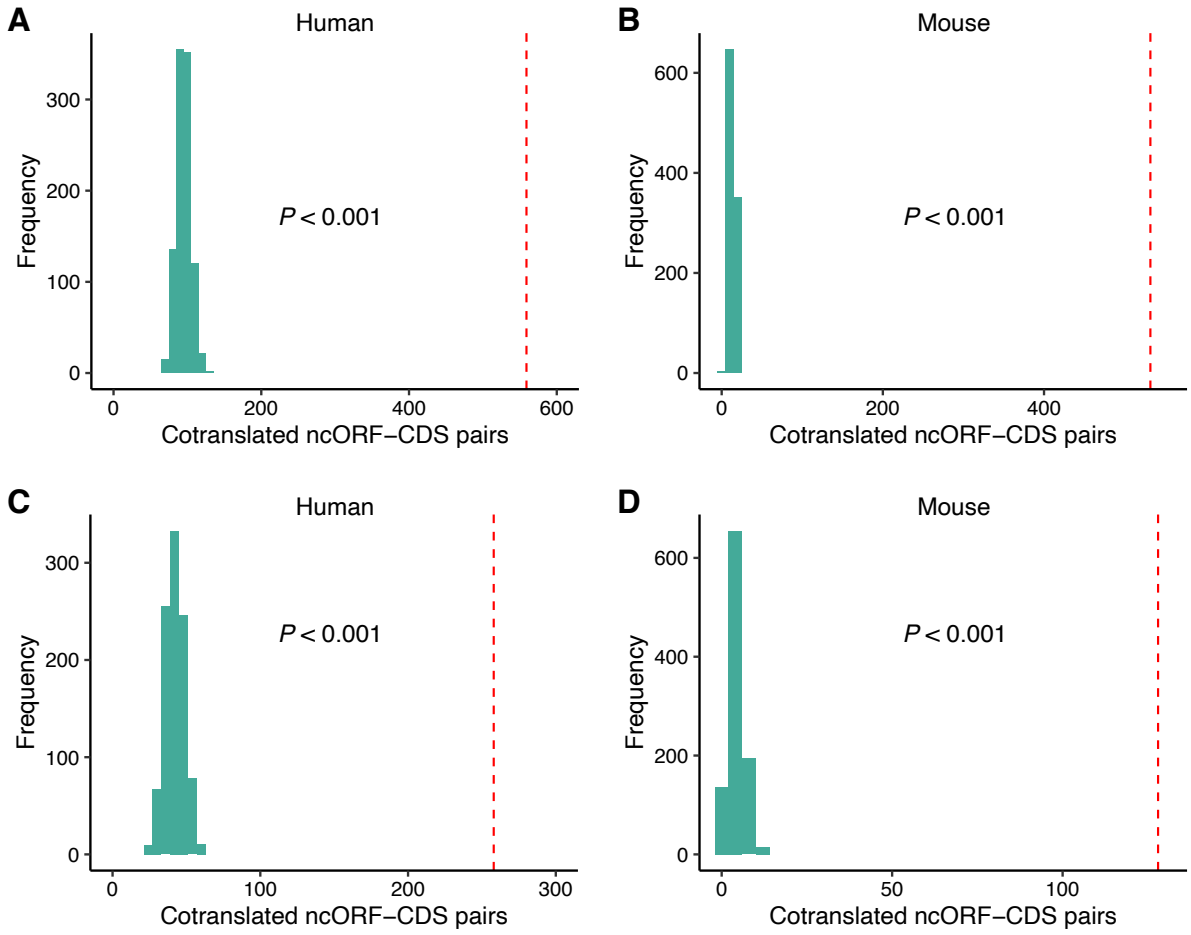

Supplementary figure 15. Permutation tests assessing co-translation between ncORFs and main CDSs within the same genes. (**A-B**) Distribution of the number of ncORFs that co-translate with corresponding main CDSs of the same genes in humans (A) and mice (B) based on the permutation analysis. Red dashed lines mark the observed counts. Empirical *P* values were indicated. (**C-D**) Same analyses as in (A) and (B), but excluding ncORFs overlapping with any CDS regions. CDS, coding sequence; ncORF, non-canonical open reading frame.

Supplementary Tables

Supplementary table 1. High-quality ribosome profiling libraries used for non-canonical open reading frame annotation.

Supplementary table 2. Clusters of genomically overlapping GENCODE non-canonical open reading frames.

Supplementary table 3. List of non-canonical open reading frames annotated in this study.

Supplementary table 4. Known non-canonical open reading frames previously reported to encode functional microproteins and independently rediscovered here.

Supplementary table 5. Non-canonical open reading frames containing Pfam domains.

Supplementary table 6. Evolutionary characteristics and constraints of non-canonical open reading frames.

Supplementary table 7. List of ribosome profiling libraries used for translation quantification.

Supplementary References

1. Lei, T., Chang, Y., Yao, C., and Zhang, H. (2023). A systematic evaluation of computational methods for predicting translated non-canonical ORFs from ribosome profiling data. Journal of Genetics and Genomics *51*, 105-108. 10.1016/j.jgg.2023.08.010.